Using natural gas content of groundwater to improve the understanding of complex thermo-mineral spring systems

Margaux Dupuy, Emilie Garel, Eliot Chatton, Thierry Labasque, Alexandra Mattei, Sébastien Santoni, Virginie Vergnaud, Luc Aquilina, Frédéric Huneau

Journal Pre-proofs

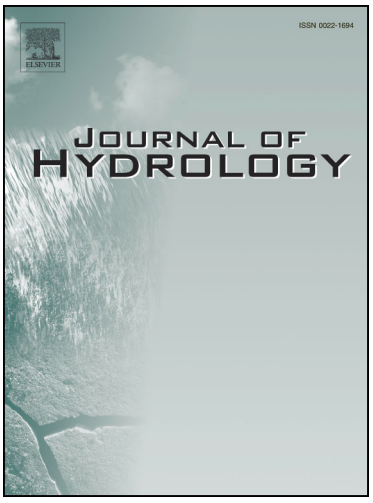

Research papers

Using natural gas content of groundwater to improve the understanding of complex thermo-mineral spring systems

M. Dupuy, E. Garel, E. Chatton, T. Labasque, A. Mattei, S. Santoni, V. Vergnaud, L. Aquilina, F. Huneau

PII: S0022-1694(24)00350-0
DOI: https://doi.org/10.1016/j.jhydrol.2024.130956
Reference: HYDROL 130956

To appear in: *Journal of Hydrology*

Received Date: 5 June 2023
Revised Date: 6 February 2024
Accepted Date: 9 February 2024

Please cite this article as: Dupuy, M., Garel, E., Chatton, E., Labasque, T., Mattei, A., Santoni, S., Vergnaud, V., Aquilina, L., Huneau, F., Using natural gas content of groundwater to improve the understanding of complex thermo-mineral spring systems, *Journal of Hydrology* (2024), doi: https://doi.org/10.1016/j.jhydrol.2024.130956

Using natural gas content of groundwater to improve the understanding of complex thermo-mineral spring systems

M. Dupuy[1,2,*], E. Garel[1,2], E. Chatton[3], T. Labasque[3], A. Mattei[1,2], S. Santoni[1,2], V. Vergnaud[3], L. Aquilina[3], F. Huneau[1,2]

[1] Université de Corse Pascal Paoli, Département d'Hydrogéologie, Campus Grimaldi, BP 52, 20250 Corte, France.

[2] CNRS UMR 6134 SPE, BP 52, 20250 Corte, France.

[3] OSUR - Plateforme Condate Eau, CNRS - Univ Rennes, Géosciences Rennes UMR 6118, 35000 Rennes, France

* now at CSIRO, GPO BOX 2583, Brisbane, QLD 4102 Australia (Margaux Dupuy) margauxdupuy@yahoo.fr,

Abstract

The varied gaseous composition of thermo-mineral waters emerging in a non-active zone reflects the diversity and complexity of groundwater pathways and provides important insights into their hydrogeological behaviours. The investigated geochemical content of complex thermo-mineral springs revealed the need to use dissolved gas contents as part of a multi-tracer approach to discriminate processes, geogenic (water-gas-rock interactions), abiotic (geological confinement, flow paths) and biotic activity influencing geochemical of groundwater along regional pathways. Irrespective of the dissolved element content or the water type, examining the overall concentration of dissolved gases enables an effective delineation of regional groundwater flow paths. Using dissolved gas content further contributed to the circumvention of some analytical challenges associated with conventional isotopic or geochemical techniques, often linked to the high concentration of elements such as iron, sulfate, sulfide or other naturally occurring elements content. The primary objectives are to analyse the gas composition of individual springs, to identify the origin of these gases in the groundwater, and to use this gas composition to improve the understanding of the flow patterns contributing to the geochemical diversity observed at the surface of the groundwater. From field investigations in a geologically and structurally complex area of Eastern Corsica (France), three types of gas contents are identified: (type 1) CH_4 & H_2S-rich, (type 2) N_2-rich and (type 3) CO_2-rich. The study of these dissolved gases highlights that the wide geochemical diversity of thermo-mineral waters observed here is not only related to the mineralogical composition of the local aquifer but also involves strong and cumulative interactions along deep regional circulation pathways. This approach also reveals a common deep crustal gaseous influence characterised by N_2 production, which interacts during up flow with groundwater and then with the local metamorphic or sedimentary rock matrix. The groundwater's isotopic and geochemical contents are then altered by local lithologies encountered through both abiotic and biotic interactions. Finally, at shallow depths, phreatic groundwater can add its geochemical and isotopic footprint and dilute this complex mixture before groundwater emerges as mineral spring. This paper answers the primary objectives yet further demonstrates that using dissolved gas as a tracer of groundwater flow paths allows a deeper interpretation of surface geochemical and isotopic observations, distinguishes local from regional flow paths, and provides information about processes at the origin of groundwater diversity.

The combination of tools presented in this paper (i.e., geochemical, dissolved gas, and isotopic tools) allows the establishment of a reliable regional groundwater flow scheme for thermo-mineral waters in a non-active zone. This scheme is essential to improve thermo-mineral water management, and protection to ensure their sustainable quality in front of increasing anthropogenic and climatic pressures.

Keywords

Hydrogeology, thermo-mineral waters, water stable isotopes, water-rock interactions, dissolved gases (CO_2, CH_4, H_2S, N_2, He)

1. Introduction

Abundant in thermo-mineral springs, dissolved gases discharged at the surface by groundwaters provide important information about hydrogeological system functioning (Giggenbach, 1991). Widely used as tracers in tectonically active zones in volcanic areas, and seismically-active regions (Werner *et al.*, 2022; Karolytè *et al.*, 2019, 2017; Bräuer *et al.*, 2017; Benavente *et al.*, 2016; Ruzié *et al.*, 2013; Mörner and Etiope, 2002), gas emission monitoring is underused as a basis for understanding the hydrogeological functioning of complex hydro-systems that are not linked to an active zone. Some studies reveal that gas discharge could not only be related to regional geotectonic settings but also the result of water-rock interactions or biotic processes occurring through topographical and hydrogeological discontinuities (Lee *et al.*, 2021; Tassi *et al.*, 2020; Kotowski *et al.*,2019, Agnew and Halihan, 2018; Amaral *et al.*, 2017).

As shown by Sacchi *et al.* (2022), to improve the sustainable management of mineral water springs, it is necessary to identify processes occurring along the flow path of valuable springs (i.e. exploited as spa or bottled). For this purpose, geochemical and isotopic tools are the only two tools generally used to characterise mineral waters (Sacchi *et al.*, 2022; Lee *et al.*, 2021; Lavrushin *et al.*, 2018).

Nevertheless, the dissolved gas content can provide valuable information about the subsurface flow system by significantly contributing to understanding the origin of flow through the escape mechanisms of natural fluids. Preferential water flow through tectonic structures is responsible for pressure variation, consequently triggering the progressive release of gas at the surface as a function of their solubility. In the non-active zone, some studies have revealed that gas-rich waters are only generated by meteoric water infiltration and groundwater rocks interactions even in the shallowest part of the crust (Agnew and Halihan, 2018). Subject to the natural increase in temperature with depth, waters are warmed and, then flow through and between geotectonic units. The latter are preferential pathways that allow water to quickly reach the surface before losing heat (Goswami *et al.*, 2022; Craw *et al.*, 2013; Grasby *et al.*, 2000). Physical and chemical alterations due to depth associated with geological and geotectonic conditions can increase water rock interactions and lead to gas release (Štrbački *et al.*, 2020). From the respective proportions of dissolved carbon dioxide (CO_2), methane (CH_4) or nitrogen (N_2) combined with the proportion of reactive (H_2, H_2S, etc.) or noble (He, Ne, Ar) gases measured in groundwater, processes causing their release could be identified (Agnew and

Halihan, 2018). Apart from atmospheric origin, the dissolved CO_2 has various origins such as deep-seated mantle (magmatic influence), thermogenic or biogenic (both occurring in sediments). Well known as anthropogenic emission (i.e. landfill, agricultural activities, etc.), the greenhouse gas CH_4 has multiple natural origins such as volcanic and, wetlands and or could be also the evidence of biotic processes from an anaerobic environment where microbial fermentation of organic matter occurs. The last major gas found is N_2, which may have an atmospheric origin, a magmatic origin, or can be caused by the intrusion of deep fluid. According to their potential origin and to their geochemical and isotopic composition, groundwater samples collected at the surface can provide information about fluid origin, up-flow paths and reservoir interactions with geological matrixes (D'amore *et al.*, 1987). To ensure the sustainability of this mineral groundwater, gas monitoring was revealed to be a powerful and innovative tool to identify hydrochemical processes at the origin of springs, and to conceptualise the whole hydrogeological system as well as the aquifer conditions of flow paths. This study aims to use dissolved gases as integrative tracers of the water pathways within a non-active zone and regardless of the geological context or geological unit encountered (Marques *et al.*, 2020; 2000 Tassi *et al.*, 2020; Angelone *et al.*, 2005; Minissale *et al.*, 2019, 2004, 1999; Michard, 1990).

Corsica Island (France), and particularly its eastern part, highlights a wide hydrochemical diversity of thermo-mineral waters (Na-HCO_3, Ca-HCO_3, Ca-SO_4- HCO_3 and Na-Cl), not linked to any seismic- or tectonic activity (Dupuy *et al.*, 2021). Emerging from a small mountain-plain continuum (<16 km), at the interface of sedimentary, metamorphic and igneous rocks, eastern Corsica thermo-mineral groundwater diversity is evidence of the existence of complex flow patterns and thus a perfect site for detailed investigations on groundwater gaseous content. To improve the gap in knowledge regarding the origin of the gas diversity observed, noble gases (He, Ne, Ar) and reactive gases (CO_2, N_2, H_2S, CH_4, H_2, O_2) were monitored to test the potential of dissolved gases to improve the hydrogeological understanding of 22 mineral springs.

The main aims were (1) to describe the gas composition of each spring; (2) to characterise the origin of these gas phases in groundwater and to differentiate geogenic from biotic influences. Then, using this gas composition (3) improves the description of the flow patterns involved in the groundwater diversity observed at the surface.

This work provides significant information regarding the major interest in investigating the gaseous phases of groundwaters in non-active zones, taking advantage of the complex hydrogeological model offered by Corsica Island geological conditions.

2. Study area

120 Localisation and hydroclimatology

121 In the Western Mediterranean Sea, Corsica Island (France) has a contrasted topography
122 (up to 2706 m. above sea level – asl.). The investigated area, located on the eastern part of
123 the island extends over 1,500 km². In the west of the study area, a mountainous zone, of
124 1034 km², rises to 2136 m, while in the east, the coastal part is a lowland plain extending
125 over 466 km². Despite the typical Mediterranean climate of the island, the mean
126 temperatures and precipitation vary significantly with the altitude (Fig. 1). According to
127 Bruno *et al.* (2001) average annual precipitation increases from about 600 mm near the
128 coast to more than 1600 mm at 1500 m asl, while the mean annual temperature decreases
129 from 16°C near the coast to 10°C at 1500 m asl (Mattei *et al.*, 2021; Bruno *et al.*, 2001). These
130 observations are confirmed by the ombrothermal diagrams displaying precipitation and
131 temperature observed on 3 cities of the study area, at Corte at 429 m asl (inland), Bastia
132 and Solenzara, two lowland stations respectively at 1 and 12 m asl . The inland part is
133 characterised by alpine climate conditions with high snowfall in winter and storm rain
134 events during the driest months from May to September for inland stations (Fig. 1) (Mattei
135 *et al.*, 2021; Rome and Giorgetti, 2007). While lowland stations saw their driest months
136 from April to September (Fig. 1). The study area is drained by four main rivers flowing
137 from West to East: the Solenzara River and the Travu River in the south part, the
138 Tavignanu River and the Golu River in the northern part (Fig. 2).

139 Geological and hydrogeological overview

140 The study area is located at the interface of 4 main geological units on the island (Fig.
141 2) (Caritg, 2009a, 2009b). The basement, mainly made of calc-alkaline granitoid rocks from
142 the Hercynian orogenesis, extends over the south-west. It is overlapped, along an N.NW-
143 S.SE axis, by two units from the Alpine orogenesis; the first unit is Eocene flysch, an
144 autochthonous sedimentary detrital unit and the second is lustrous schists, an
145 allochthonous metamorphic unit also called 'Alpine metamorphic unit', observed only in
146 the 'Castagniccia region'. The Neogene sedimentary basin of the Aleria plain is separated
147 from the allochthonous units by the Saint Antoine fault N.NE-S.SW oriented (N020°)
148 (Loÿe-Pilot *et al.*, 2004). Geological and hydrogeological information of each unit
149 encountered in the study area is detailed in the paragraphs below.

150 In the study area, the Hercynian basement is mainly composed of biotite-rich
151 monzogranite, tonalo- or monzogranodiorite (Rossi *et al.*, 2015; Caritg, 2009a, 2009b). The
152 Pietrapola springs (Fig. 2) flow out of monzogranite in which alkaline feldspar [Na, K]
153 and plagioclase dominate [Na, Ca]. In the Travu valley, the Caldaniccia spring (Fig. 2)
154 flows out of tonalogranodiorite and monzogranodiorite, with plagioclase feldspars
155 dominant over alkaline feldspars, biotite [K, Mg, Fe, F] and amphibole [Ca, Mg, Fe]. The
156 granitic basement is intensively fractured by NE-SW faults (Caritg, 2009a). Only a few

reports from the French geological survey exist and they provide basic information on groundwater flows and aquifer capacity of this unit (Caritg, 2009a, 2009b). As in a mainly hard rock context, deep fractures associated with the superficial weathered horizon are the most favourable zones for the groundwater circulation and aquifer capacity (Lachassagne, 2011; Genevier *et al.*, 2011; Dewandel *et al.*, 2011; Caritg, 2009a; Caballero *et al.*, 2006).

The Alpine metamorphic units are derived from the exhumation of oceanic and continental tectonic units involved in the Alpine orogeny (from the Late Cretaceous to the late Eocene, *e.g.*, (Di Rosa *et al.*, 2017). These tectonic units include metamorphic granitoids and metamorphic sedimentary rocks with metamorphic rocks derived from the oceanic crust (serpentinites, metagabbros and metabasalts). The observed so-called 'Lustrous schists' display a wide range of metamorphic facies from blueschist facies (mainly Inzecca series), eclogite facies (mainly Serra di Pigno and Castagniccia series) to greenschist facies (Piccoli *et al.*, 2018; Gueydan *et al.*, 2017; Di Rosa *et al.*, 2017; Vitale Brovarone *et al.*, 2013; Caritg, 2009b). These units are intensively folded and characterised by discontinuities displaying an NS orientation of schistosity, creating favourable hydrogeological conditions for many springs in the Castagniccia region (Fig. 2).

The Eocene autochthonous flysch is a vertical alternation of conglomerates, sandstones and dark clay, mainly made of arkose and pelite rocks. This formation rubs up against the Hercynian basement along the NE-SW contact and is overlapped by sedimentary deposits in the eastern part (Berthier *et al.*, 1980; Amaudric, 1973). Vignola springs from the Travu Valley, Fontanella and Acqua acetosa are springs flowing out at the interface of this heterogeneous unit known as a low aquifer potential area (Caritg *et al*, 2009b).

The Neogene sedimentary formation is heterogeneous: from breccias and conglomerates to sands and marls. Due to basin subsidence, Neogene deposits dip to the east with an approximate thickness of 2 km at the coastline and up to 8.5 km in the middle of the Corsican channel. Covered by thin Quaternary alluvial deposits (Fig. 2), they are cut by N145-N155 and N20-N30 faults. These Neogene sediments present a few shallow local aquifers with very low productivity. However, their thickness and lithologic diversity suggest a noticeable hydrogeological potential as a deep multi-layer aquifer supported by the occurrence of artesian boreholes (Serrano *et al.*, 2013; Loÿe-Pilot *et al.*, 2004).

Hydrochemical background of springs in the study area

Twenty-four thermo-mineral springs flow out at the interface of the main geological formations described above (Fig. 2). Dupuy *et al.* (2021) the 6-month sampling campaign in 2018 provides a first overview of hydrochemical characteristics of 19 thermo-mineral

groundwaters and results are summarised below.

The Pietrapola and Caldaniccia sites show springs flowing out respectively from potassium feldspar-rich- monzogranite and tonalograniodiorite. Thereby a high-altitude recharge (>800 m asl) supplies the springs emerging through major faults providing thermal-alkaline-water, fully equilibrated with rock. Their low mineralisation (<300 µS/cm) associated with a Na-HCO_3 water type and high SiO_2 content confirms that this water is provided by the hydrolysis of Hercynian granitoids at depth (Dupuy *et al.*, 2021).

All other springs are cold resulting from a local recharge at a shallower depth. Acqua acetosa, Vignola and Fontanella flow out at the interface between Eocene Flyschs and Hercynian basement or Neogene sediments (Table 1). These 3 springs are highly mineralised (from 2100 and up to 12 000 µS/cm²), contain high levels of chlorine, boron and fluorine and display respectively a Ca-Na-HCO_3 for Acqua acetosa and a Na-Cl water type for the latter two. Their high mineralisation comes partly from the dissolution of interstitial-residual-brines (Aquilina *et al.,* 2011). This geochemical diversity translates to the importance of tectonics in the complexity of the flow pattern involved at the interface of the different geological units (Martín-Loeches *et al.*, 2020).

The Puzzichellu springs group flows out along the Saint Antoine fault, aligned on a N20-N30 axis (Fig. 2), where the Puzzichellu and the Campo-Favajo springs emerge from sandstones including rhyolite conglomerates covered by deposits of organic matter-rich marls (Caritg *et al.*, 2009a, 2009b). This group is characterised by Na-HCO_3, Ca-Na-HCO_3 and Ca-SO_4- HCO_3 water types. Here, deep groundwaters are influenced during the upflow process by mixing with more carbonated groundwaters of sedimentary origin (Dupuy *et al.*, 2021). The sulfur isotopes performed on the artesian borehole of the Puzzichellu site (PUZ-F, Table 1) have shown the presence of bacterial activity, explaining the high sulfate and sulfite content recorded in the groundwater (Dupuy *et al.*, 2021; Dominici *et al.*, 1986).

3. Sampling and analytical procedures

3.1. Sampling strategy and rainfall data

Based on their legal accessibility, geology and spatial coverage 22 thermo-mineral waters, located at 15 different sites and flowing out at low altitudes (<554 m asl) were sampled. The location, name and exact geographical coordinates are provided in Table 1.

To identify altitude recharge of precipitation at a regional scale, $\delta^{18}O$ and $\delta^{2}H$ extracts from a monthly sampled precipitation observation network at 5 stations [Aleria (9 m), Bastia (1 m), Bonifacio (99 m), Corte (486 m), Campana (760 m), and Palneca (785 m)] were

used to calculate the isotopic altitudinal gradient from data extracted from Nlend B. *et al.*(2023)and Mattei *et al.* (2021). By calculating the linear regression relating the rainwater stable isotope values to their sampling altitude, a regional isotopic elevation gradient can be obtained; here considered equal to $\delta^2H = -0.019 * altitude\ (m\ asl) + (-34.876)$. This equation can be used to estimate the recharge altitude of springs out on the eastern part of the island.

3.2. Groundwater sampling procedures

The 22 springs were sampled monthly from January 2018 to March 2019. Physical and chemical parameters were simultaneously measured in the field. Electrical conductivity (EC), temperature (T), redox potential (Eh) and pH were measured with a WTW multi 3410 (WTW gmbH, Weilheim, Germany). Bicarbonates concentration (HCO_3) was also determined, in the field, using a HACH digital titrator (HACH Company, Loveland, USA). Samples were filtered through 0.45 µm nitrocellulose membranes for determination of major ions and stored in two 50 mL polyethylene bottles before storage at 4°C. One bottle was acidified using ultrapure nitric acid for cation analysis. A Dionex ICS 1100 chromatograph (Thermo FischerScientific, Waltham, USA) was used to determine ionic concentrations at the Hydrogeology Dept. of the University of Corsica (CNRS UMR SPE 6134). The analysis was checked and validated for ionic balance under 10%.

For the stable isotopes of the water molecule analysis ($\delta^{18}O/^2H$), 20 mL amber glass bottles were filled without filtration and no headspace to ensure perfect conservation then were stored at 4 °C. They were determined using a Liquid-Water stable isotope analyser DLT-100 (Los Gatos Research, San Jose, CA, USA) at the Hydrogeology Department of the University of Corsica (CNRS UMR 6134), France, following the analytical scheme recommended by the IAEA (Penna *et al.*, 2010). The analytical precision was better than 0.5‰ for ^2H and 0.2‰ for ^{18}O.

For tritium (^3H) analysis, 500 ml polyethylene bottles were filled and then stored at 4°C until analysis. The ^3H activity was measured by a liquid scintillation analyser (DL > 0.2 UT) following the protocol of Thatcher et al (1977). These analyses were carried out at the Hydrosys Labor Kft. in Budapest, Hungary.

3.4. Gas sampling procedures

During four campaigns in 2018 (April, July, September, and December), springs were also sampled for the analysis of dissolved gases in 500 ml glass bottles by over-flushing, after rinsing three times the bottle volume with the spring water. Bottles were closed with rubber caps and sealed with a metal ring, then sent within 48 hours for analyses at the

Geosciences Rennes laboratory (CNRS UMR 6118) as detailed in Chatton *et al.*, 2017. Noble and reactive gases (Ne, He, Ar, N_2, O_2, CO_2) were extracted by headspace and measured by gas chromatography equipped with a catharometer detector (μGC 3000 – SRA) at the Condate Eau platform (OSUR CNRS - Univ Rennes, France). Uncertainty is estimated at +/- 5% for [CO_2] and [CH_4] and +/- 3% for other gases.

The anthropogenic gases (CFCs and SF_6) were sampled in stainless-steel ampoules after washing through at least three volumes of the ampoule and before closing it to ensure no air contamination. Their concentrations in groundwater were obtained through a methodology of purge-and-trap inspired by Busenberg et Plummer (1992). Water was degassed by N_2 stripping and gases were trapped in a stainless-steel tube filled with HayesepD® and maintained at −100 °C in an ethanol bath. After 6 (CFCs) or 10 (SF_6) min of pre-concentration, the gases were injected into a Gas Chromatograph equipped with an Electron Capture Detector (GC–ECD, Perkin Elmer) by immersing the trap into boiling water. The analytical uncertainty is estimated to be 1–3% for CFCs and near 5% for SF_6. Analyses were performed at the Condate Eau Platform (OSUR CNRS-Univ Rennes, France).

3.5 Recharge condition modelling

Dissolved gases, such as argon (Ar), nitrogen (N_2) and neon (Ne), were used to model recharge conditions, using an inverse model developed from the methods described by Aeschbach-Hertig *et al.* (1999). This model has been adapted to use the available dissolved Ne, Ar and N_2 concentrations in cm^3STP/g (Standard Temperature and Pressure) to model the Temperature (NGT) and the amount of excess air (EA) as already applied on hydrogeological systems by Chatton *et al.* (2017). Limited by the low quantity of available dissolved gases (Ne, N_2 and Ar) and their related analytical uncertainty, this study considers a simple model of excess air formation to determine the recharge conditions (NGT and EA). The established inverse model is established considers an Unfractionated Air model (UA model), which assumes a total dissolution of unfractionated excess air during the recharge. That means that the reverse model will consider that dissolved noble gas concentrations depend on different parameters: the recharge temperature (so-called noble gas temperature, NGT), the volume of unfractionated excess air (EA), the altitude of recharge and the recharge salinity. The two latter field parameters being known, only two free parameters (NGT and EA) remain to be determined using the inverse model with a degree of freedom $\nu = 1$. Because absolute NGT values were not conclusive, only the Excess Air (EA) concentration was used in this paper and results are displayed in Table 3.

3.6 Statistical analysis: Principal component analysis (PCA) and Hierarchical clustering (HCA)

A Principal Component Analysis (PCA) is a statistical technique used for a dimensionality reduction of input data in order to simplify data visualisation. In our study, PCA is applied to identify patterns and relationships within complex datasets of variables such as physicochemical parameters (pH, Eh, T, E.C), geochemical components (HCO_3) and gas contents (O_2, CO_2, CH_4, H_2S, N_2, He, Ne, Ar, H_2) and displaying it by springs. It allows us to represent the data in a lower-dimensional space, facilitating the interpretation of underlying patterns (Everitt, B.S., 2001, Kim, K.-H, 2020).

A heatmap generated by Hierarchical Cluster Analysis (HCA) visually represents the results of clustering analysis. In the context of HCA, a heatmap displays a matrix of colours where each cell corresponds to a pair of variables or observations. The intensity of the colour in each cell indicates the degree of similarity or dissimilarity between the paired variables or observations. Clusters of similar entities are visually apparent as contiguous blocks of similar colours, providing a clear representation of hierarchical relationships within the dataset. Heatmaps are valuable for identifying patterns, trends, or groupings in complex datasets analysed through HCA. In our study, according to the methodology displayed by Tarvainen (2019), HCA is employed to categorise gas abundance in springs into hierarchical structures, aiding in the identification of distinct groups within the dataset.

4. Results and discussion

4.1. Water type diversity

During the sampling period, the groundwater temperature ranges from 11 to 54°C distinguishing thermal waters (T>20°C), such as at the Pietrapola site and the Travu valley (N = 8), from cold waters (T<20°C) which concerns all the other springs (N = 14, Table 1). A wide range of mineralisation levels and pH values are observed ranging from 150 µS/cm (CALD) to 12 620 µS/cm (FONT) with pH ranging between 4.45 (S-SUP) to 9.7 (P-LAV) (Table 2). In order to discriminate water types, major element proportions were displayed on a Piper diagram (Fig. 3). Three main water types are observed Na-Cl, Na-HCO_3 and Ca-HCO_3, also with two intermediate facies Na-Ca-HCO_3 and Ca-SO_4-HCO_3. Thermal waters at the Pietrapola site and CALD, show a typical Na-HCO_3 water type affirming their geothermal origin from granitoid rocks (Fig. 2) (Martín-Loeches *et al.*, 2020). The thermal spring VIGN and the cold spring FONT, have a Na-Cl water type; this mature water (Giggenbach, 1988) shows long-time interaction with detrital rocks. The Ca-HCO_3 water type is observed for all the Castagniccia Region springs (Fig. 2, 3) except S-SUP, which displays an intermediate Ca-SO_4-HCO_3 water type, PORT and FAJO-G displaying another intermediate facies Na-Ca-HCO_3.

Springs located on the sedimentary plain show diversified water types: CAM-F with a

Na-HCO_3 water type is close to waters flowing through granitic rocks; ACQ has an intermediate facies Na-Ca-HCO_3 characteristic of groundwaters flowing at the interface of magmatic and sedimentary rocks (Martín-Loeches *et al.*, 2020); then the Puzzichellu site shows two springs with another intermediate Ca-SO_4-HCO_3 water type.

Thus, the geochemical signature of the thermo-mineral springs highlights five different groundwater types, representing a high diversity of springs for a small area. These five water types (Fig. 3) and their spatial distribution (Fig. 2) are not correlated with the geological unit from which they spring out.

4.2. Water gas composition

4.2.1. Multi-criteria classification of gaseous discharge

To improve the understanding of groundwater flows and to discriminate the origin of the various geochemical signatures, a multi-criteria classification of gaseous discharge composition was carried out by applying hierarchical cluster analysis (HCA) on chemical abundance gas measured in April, September and December 2018 (Table 3). In Fig. 4, the average gas concentration by spring is depicted according to colour from low concentration (dark blue) to high concentration (deep red). Hierarchical cluster analysis is performed on the 13 thermo-mineral groundwater samples, based on 9 dissolved gas components (Ne, He, Ar, N_2, H_2, CO_2, O_2, CH_4, H_2S) and indicates the existence of only three clusters with three distinct gaseous types: Type I (CH_4 and H_2S), Type II (N_2) and Type III (CO_2). Visual inspection of the vertical dendrogram reveals that cluster 1 is linked to the remaining two other cluster types at a great distance, indicating that the gaseous origin of Type I differs strongly from the rest of the analysed groundwater. Each related cluster and main gas composition is detailed below.

4.2.1.1 Type I: CH_4 and H_2S rich springs

Cluster 1 concerns a borehole (PUZ-F) and a natural water spring (CAM-F) flowing out from the Neogene sedimentary depositions (Fig. 2). These groundwaters are intermediately mineralised (1041< E.C.<1592 µS/cm), neutral to alkaline (6.9<pH <8, mean value 7.3), with varying water types due to major ions showing natural variations (Fig. 3): from Ca–HCO_3-SO_4 in PUZ-F to Na–HCO_3 in CAM-F. Temperatures are below 20°C (13.5< T(°C) <17.5) and a typical smell of hydrogen sulfide (rotten egg) is very strong at both sites. Springs concerned by the Cluster I are characterised by the highest concentration in CH_4 and H_2S measured in the study area with an average CH_4 concentration of $9*10^{-4}$ mol/l (PUZ-F) up to $2*10^{-3}$ mol/l (CAM-F) and an average H_2S concentration of $1*10^{-4}$ mol/L (PUZ-F) to $4*10^{-5}$ mol/l (CAM-F) (Table 3, Fig. 4). The average H_2 content ($1*10^{-8}$ mol/l) measured in CAM-F is noticeable. The average CO_2 content varies from $1*10^{-3}$ to $3*10^{-4}$

mol/l, for CAM-F and PUZ-F respectively, and it is associated with the very low amount of O_2 (respectively from $3*10^{-7}$ to $5*10^{-7}$mol/l) these concentrations suggests that the water flows mainly through anoxic environment. Type I also highlights the occurrence of significant content in Ne, Ar and N_2 respectively up to $9*10^{-9}$, $2*10^{-5}$ and $7*10^{-4}$ mol/l, which are characteristic of the next cluster (Type II: N_2-rich springs) (Fig. 4).

4.2.1.2 Type II: N_2-rich springs

This second cluster concerns thermal springs (CALD, P-SOA, P-LAV, P-B), characterised by alkaline pH above 8.7 up to 9.7, very low mineralisation (mean value ≈330 µS/cm) and temperatures ranging from 30.4 to 54.7°C (Table 2) with Na and HCO_3 as dominant ions in all samples. This type is mainly represented by a high content in N_2 between $4*10^{-4}$ and $6*10^{-4}$ mol/l associated with noble gas occurrence Ne (up to $8*10^{-9}$ mol/l), Ar (up to $2*10^{-5}$ mol/l) and He (up to $8*10^{-7}$ mol/l) (Fig. 4).

4.2.1.3 Type III: CO_2-rich springs

The third cluster corresponds to the cold carbonated waters of Castagniccia and to two springs (FONT and ACQ) emerging in the sedimentary plain. These springs show temperatures ranging from 11°C (AMPU) to 22°C (ACQ), with a wide range of mineralisation from 230 µS/cm (S-SUP) to 2 890 µS/cm (ACQ) and up to 12 620 µS/cm (FONT) (Table 1). The Ca–HCO_3 water type is the dominant feature, even if a Na-Cl water type is observed at (FONT). This type presents a very high content in CO_2 with concentrations varying between $2*10^{-2}$ and $4*10^{-2}$ mol/l associated with N_2 occurrence up to $4*10^{-4}$ mol/l (Fig. 4).

4.2.2. Abundance classification

Three main gaseous provinces have been identified from the multi-criteria classification of gaseous discharge performed on the thermo-mineral groundwaters: CH_4 and H_2S-rich (Type I), N_2-rich (Type II), and CO_2-rich (Type III). According to Faramawy *et al.* (2016), natural gas flux may have multiple origins and come from different processes such as, thermogenic processes forming CO_2, H_2S, H_2 and N_2, abiogenic processes forming CH_4 from mantle degassing or CO_2-reduction (Sherwood Lollar *et al.*, 2002; Rojey, 1997), but also from biogenic processes forming CH_4, CO_2 and H_2. In addition, two processes could also participate at the same time and provide the same gas content, as has already been observed in different regions (Štrbački *et al.*, 2020; Barros *et al.*, 2020; Moritz *et al.*, 2015; Angelone *et al.*, 2005; Sherwood Lollar *et al.*, 2002).

As shown in Fig. 4, each type representing the major gas released is also associated with minor gases that are also released at the same time. The relative occurrence between

major and minor gas occurrence gives information about the processes involved, flow patterns or combination processes occurring along flow paths. Indeed, the occurrence of dissolved gases in groundwater is often the result of flow pattern mixing (Lee *et al.*, 2021; Hiscock, 2009; Kipfer *et al.*, 2002). Influenced by physical degassing processes, these minor gases appear in relative proportions as follows: N_2, Ar and Ne for Type I (CH_4 and H_2S-rich), Ne and Ar with He for Type II (N_2-rich) and N_2 for Type III (CO_2-rich) (Fig. 4). This observation highlights a minimal proportion of N_2 in each Type and the occurrence of Ar and Ne in Type I and II. However, further study of the amount of dissolved gas is needed to determine their origin.

4.2.3. Gas origin

To relate the composition of gases with their potential genesis processes, the 100*N_2-CO_2-10000*Ar and the N_2-1 000*He-100*Ar ternary diagrams, proposed by Giggenbach *et al.* (1983) and established from Powell and Cumming (2010), are shown in Fig. 5. This figure displays groundwater dissolved gas content according to their relative content in N_2, Ar, CO_2 (Fig. 5.A) and N_2, Ar, He (Fig 5.B).

In Figure 5.A, the trend towards the CO_2-vertex highlights the high amount of CO_2 contained in Type III springs and shows its seasonal degassing processes. The gas content varies according to the month of sampling. This trend also shows that CO_2 content is not linked to volcanic or to magmatic phenomena.

The literature highlights that the thermal decomposition of organic matter involves alteration of the ^{13}C-CH_4 isotopic signal varying from -60‰ to -20‰ (Faramawy *et al.*, 2016; Whiticar *et al.*, 1986; Berndt *et al.*, 1996). In contrast to abiogenic processes responsible for the reduction of CO_2 into CH_4, mainly observed in hydrothermal water-rock interactions and serpentinization of ultramafic rocks (Sherwood 2002), which shows an enriched signal ^{13}C-CH_4 > -60‰ (Agnew and Halihan, 2018; Faramawy *et al.*, 2016). Biogenic processes due to biotic activity are responsible for gas production and show a depleted ^{13}C-CH_4 <-60‰ signature. In the regional literature, the $\delta^{13}C$-CH_4 signature was performed on 3 carbo-gaseous springs of Castagniccia (Type III) and revealed an accurate $\delta^{13}C$-CH_4 isotopic ratios of -26.1 (AMPU), -24.9 (PORT) and -21.6‰ (MOIT) (Berthier *et al.*, 1980). This signature is usually indicative of thermogenic processes corresponding to a slow decomposition of organic material with depth because of an increase in pressure and temperature on sedimentary rocks (Barros *et al.*, 2021, Faramawy *et al.*, 2016; Berndt *et al.*, 1996; Whiticar *et al.*, 1986). As observed in thermo-mineral waters from Italy by Minissale (2004), a CO_2 content which comes from mantle degassing is added, along the groundwater pathway, thermogenic- CO_2 coming from the remobilisation of metamorphic decarbonation reactions of carbonated rocks (Barros *et al.*, 2021; Lavrushin *et al.*, 2018; Petrović *et al.*, 2010; Thiébaud *et al.*, 2010). During the metamorphism of

sedimentary rocks, calcite reacts with SiO_2-rich fluids to produce wollastonite rock and CO_2. The latter is then trapped by the schistiosities of the rocks (Chiodini *et al.*, 2020). Some wollastonite deposits were identified in Castagniccia and allow confirmation that the high CO_2 content here is an addition of thermogenic CO_2 to mantle-degassing CO_2 (Vitale Brovarone *et al.*, 2013; Malvoisin *et al.*, 2012; Ravna *et al.*, 2010).

The two figures (Fig 5.A and 5.B) highlight that all thermo-mineral groundwaters encountered have an N_2/Ar ratio ranging between air and air-saturated water (ASW) ratios. This ratio suggests that the N_2 component comes from trapped air, due to atmospheric gases solubilised during rain infiltration (Fig. 5.B) (Epstein *et al.*, 2021, Powell and Cumming, 2010; Minissale, 2004; Rojey, 1997; Giggenbach *et al.*, 1983). The relatively higher content in Argon can be explained by radiogenic decay accumulating along flow paths and translating long residence times, confirming previous isotopic dating results (Dupuy *et al.*, 2021). Moreover, some studies also reveal that Ar could be also produced by bacterial consumption of oxygen stock in an organic-rich environment. This process added to water with a relatively shorter residence time could explain why the highest Ar-content is observed during September, in PUZ-N and CAM-F springs, both emerging from a rich organic matter environment (Faramawy *et al.*, 2016, Rojey *et al.*, 1997). As observed on neighbouring Sardinia island, N_2-rich waters are aligned along the ASW - Crust axis suggesting a general increase in crustal He produced by radioactive decay (Fig 5.B), mostly observable during the winter period (Amaral *et al.*, 2017; Minissale, 2004; 1999; Paternoster *et al.*, 2017). Helium is a radiogenic gas, produced from the radioactive decay of U and Th present in weathered rocks from Earth's crust. Low in the atmosphere, He is widely used as a tracker of volcanic activity, translating gases' deep origin from mantle or crust degassing (Amaral *et al.*, 2017). Therefore, according to Hiscock (2009), its accumulation in groundwater could also be due to long interaction time in U-Th- rich rocks. N_2, associated with the He amount provides unequivocal evidence for a contribution of deep non-atmospheric gas to these groundwater samples and a long residence time (Casillas-Trasvina *et al.*, 2023, Zippa *et al.*, 2019, Kulongoski *et al.*, 2008).

4.3. Reactional processes

4.3.1. Processes identification

Principal component analysis (PCA) was performed from in-situ physical and chemical parameters (T, pH, Eh, O_2, HCO_3), combined with gas abundance in April 2018, to confirm the different processes occurring (Figure 6, Table 1). The first two components explain 50.35% of the total variance of the population. The component F1 is negatively correlated with high CO_2 content, showing the CO_2 degassing (Type III), and positively correlated with N_2, Ar and Ne characterising a crustal influence (Type I and Type II) (Mikhail and Sverjensky, 2014). This last observation highlights the occurrence of deep influence also

on springs from the sedimentary plain (Type I). The component F2 is positively correlated with O_2 content, highlighting mixing with surface waters concerning mainly one Type III spring (AMPU). The component F3 is positively correlated with H_2S and CH_4-content and negatively with He and Temperature; this axis differentiates biotic processes observed in Type I from water with long residence times (Type II) (Dupuy *et al.*, 2021).

4.3.2. Biogenic gas evidence

The determination of recharge conditions allows the determination of the excess air (EA) contribution. This value reflects the difference between groundwater gas concentration observed in water and modelled concentration at the recharge area (Table 3). A positive EA reflects a gas supply within the aquifer while a negative value means the involvement of degassing processes, which can be also associated with dilution processes (mixing or pressure variation due to the tectonic structure). EA determined on CO_2–free sources only, Type I and Type II, shows values ranging between $-6.24*10^{-3}$ (CAM-F) and $1.28*10^{-3}$ (PUZ-F). All springs show negative EA suggesting the involvement of dilution processes, except for PUZ-F (Type II), which shows a positive value during the whole of the sampling period. As suggested in the literature, the combination of CH_4 with a high amount of H_2S in groundwater suggests the involvement of biotic processes (Tassi *et al.*, 2020 Lavrushin *et al.*, 2018; Etiope, 2017; Gilhooly *et al.*, 2014; Dupalová *et al.*, 2012; Machel *et al.*, 2001). Associated with the ^{34}S-SO_4 and ^{34}S-H_2S data measured at the same mineral spring from Dupuy *et al.* (2021), this positive EA value confirms that those biotic processes are responsible for the increase of gas content in the aquifer, due to the biological degradation of organic matter. This spring emerges from Miocene sediments known to contain thick organic matter-rich marls (Aghione deposits of the Miocene). However, negative EA values found on other Type I groundwaters (CAM-F & PUZ-N) also emerging from the Miocene sediments are correlated with ^{34}S values measured in a previous study, which does not show significant biotic activity (Dupuy *et al.*, 2021). The EA seems therefore to be a good tracer of high biotic processes, showing equivalent results to ^{34}S analyses (Table 3).

4.3.3. Groundwater equilibration

Dissolved gas prevalence in groundwater is linked to physical and chemical parameters and element equilibration state; a pH-Eh diagram was used to characterise reservoir conditions affecting the gas content (Fig. 7, Table 2). Considering a stable pH value, the variation of Eh ranging from -238 to 401 mV represents the water equilibrium state and allows identifying equilibration with gas prevalence. All springs studied flow mainly under confined reducing conditions (Fig. 7). The CO_2 and N_2-rich springs (Type II and III) plot in the prevalence state of their predominant gas phases. Type I waters do not plots either in the CH_4 or in the H_2S prevalence area, and highlight a higher Eh value than

expected for CH_4 and H_2S rich springs. Figure 7 shows that the CH_4 prevalence area is close to the NH_4^+ predominance area .

To identify springs influenced by abiotic processes, the simple NH_4^+ occurrence in groundwater was used as a witness of the water flowing through very reducing conditions. Indeed, the NH_4^+ is naturally released from the degradation of organic nitrogen under highly reducing conditions. Its occurrence in groundwater, especially when the physicochemical parameters of springs do not align with the NH_4^+ prevalence conditions, underscores water flowing through strong geologic confinement, as observed for Type I and some springs of Type II. The NH_4^+ values ranged from 0.01 (PUZ-N) to 2.17 mg/L (CAM-F) for Type I and ranged from 0.09 (MOIT) to 1.56 mg/L (FONT) for Type III. The spring CAM-F displays the highest concentration in NH_4^+.

The fact that very reducing conditions are reached may cause a secondary production of CH_4 from CO_2, by processes referred to here as abiotic, and explain the high CH_4, CO_2 and H_2S gas content measured in some groundwaters (Fig. 8) (Tassi *et al.*, 2020; Marques *et al.*, 2018; Minissale *et al.*, 2000; Paull *et al.*, 2000). Indeed, results from Figure 7 associated which the binary diagrams (Fig. 8), allow to distinguish the gas variation involved by the biotic activity from abiotic production with the example of the CAM-F springs (Chelnokov *et al.*, 2018; Jenden *et al.*, 2015). Then, the re-equilibration of water during the up-flow under oxidative conditions explains the Eh value observed at the discharge.

4.4. Flowpath

4.4.1 From degassing to local flow information

As suggested by the high dissolved gas content and confirmed by the negative EA (Table 3), degassing processes are important in these thermo-mineral groundwaters. The degassing process can result from factors such as dilution, mixing, or the local tectonic structure. This latter can lead to variations in pressure, which, in turn, influence the release of gases depending on the solubility conditions of each gas. To discriminate dilution at one side, with modern water at another side, from mixing between two different aquifer units during upwelling, anthropogenic gas (CFC and SF_6) analyses were initially performed (Table 4). Results show that SF_6 values ranged from 0.89 (P-B) to 8.33 (FONT) pptv, 19 (PUZ-F) to 166.82 (S-SOT) pptv for CFC-12, from 88.03 (FORC) to 283.04 pptv (P-B) for CFC-11 and from 3.78(P-LAV) to 18.27 pptv (PUZ-F) for CFC-113 (Table 4). These values show a low of SF_6, CFC-12 and CFC-113 with an uncorrelated high amount of CFC-11. To explain this, it is acquired that if atmospheric contamination occurs all CFCs gases should be impacted in the same proportions (Cartwright *et al.*, 2017; Darling *et al.*,2012). So only a few natural processes could explain the relative amount of variation between CFCs as microbial breakdown or sorption, but neither of these can explain the

proportion obtained here, from springs in different geological contexts (Chambers *et al.*, 2019; Kotowski *et al.*, 2019). Moreover, according to Beyerle *et al.* (1999), these anthropogenic gases are responsive to Excess Air formation and degassing processes. Degassing processes could then explain the relative proportions observed which are inversely proportional to their AE sensitivity (Cartwright *et al.*, 2017). Even if degassing processes influence the anthropogenic gas content in groundwater, their occurrence in groundwater highlights a dilution process with modern water and should be confirmed by the ^{3}H content (Table 3).

Tritium measured in groundwater ranges from 0 (P-X) to 2.3 TU (PARD); knowing that the average ^{3}H content in Corsican rainwater is about 8 TU (Juhlke *et al.*, 2020) it can be concluded that Type I are old water diluted by modern surface waters or shallow groundwaters (characterised by the presence of anthropogenic gases, negative EA and with noticeable ^{3}H amount). By comparison, the negative AE combined with groundwater deprived of ^{3}H characterises Type II as composed of old groundwater only. Type III groundwater shows the widest diversity of flow path contributions. In this category (CO_2-rich springs) some springs are mainly composed of old water while many other springs result from mixing processes between old water diluted with an actual water fraction (Table 3) containing anthropogenic gases and ^{3}H.

4.4.2 Influence of regional flow

Noble gases found in groundwater reveal the recharge conditions history. It is usually admitted that the higher the concentration of noble gases in the water, the colder is the recharge temperatures observed (Hiscock, 2009; Kipfer *et al.*, 2002). The Ar and N_2 concentrations are displayed in Fig. 9. Carbogaseous waters (Type III) show the lowest amount of noble gas, due to their intensive degassing. Fig. 9 highlights the CH_4–rich waters (Type I) springing out from the sedimentary plain and show a higher or equivalent amount of noble gas than thermal springs (Type II). However, this observation is different from the recharge altitude estimation calculated from $\delta^{2}H$ and $\delta^{18}O$ data measured in this study (Table 2). These values show a differentiated recharge altitude ranging from 764 to 900 m asl for Type II and from 78 to 290 m asl for Type I. The noble gas concentration suggests that, even if most groundwater flow in the sedimentary plain comes from a local recharge, some springs from the plain (Type I) can also be supplied by a deeper up-flow coming from a higher altitude.

As detailed by Elena *et al.* (2020), helium is a highly volatile radiogenic gas, its accumulation in groundwater is usually proportional to the increasing depth or residence time at the contact with source-rocks (Werner *et al.*, 2022; Casillas-Trasvina *et al.*, 2022; Karolyté *et al.*, 2019; Kulongoski *et al.*, 2008). The measure of He excess is therefore significant (analytical threshold ≈ 10^{-9} cm3STP/g) due to accumulation along the flow line

and indicates very long circulatory processes. All (non-carbogaseous) springs show an excess of He. The greatest excess (from 10^{-5} and 10^{-6} cm3STP/g) is observed for Type III, however, the amount of He excess in the sedimentary plain springs (Type I) confirms their supply by the deep flow, having a long residence time.

4.4.3 Conceptual model of groundwater flow towards thermo-mineral springs

From the geochemical, the water stable isotopic and gases dataset obtained a conceptual hydrogeological model of the region is proposed (Fig. 10). It shows that meteoric water infiltrated at high altitudes (>800 m asl) infiltrates into granitic rocks through major faults and deep fractures. Water is then warmed by the natural geothermal gradient until the shallower part of the crust where water is enriched with high amounts of N_2, He, and low amounts of CO_2. The local geostructure allows the release of dissolved gases up to the near surface (Type II). However, this study reveals that the type II (N_2-rich) also supplies trough depth all other thermal and mineral springs emerging in the sedimentary plain (Fig. 11). Depending on waters and rocks encountered along the gaseous up-flow, this regional gaseous signature is locally modified by abiotic and biotic processes. During the flow path through metamorphic rocks, the deep gaseous flux is mixed with carbonated waters coming from a local recharge. The water circulation through these rocks allows the mobilisation of thermogenic CO_2 coming from metamorphosed schists (Type III). This high amount of CO_2 increases the degassing process of low soluble gases as noble gas originating from the regional gaseous flux.

Carbogaseous water also springs out in the southern part of the sedimentary plain, at the interface of the different geological units, where the metamorphosed rocks are overlapped by an impermeable geological layer of Eocene flyschs. Here also metamorphosed rocks supply the sedimentary plain at depth with N_2 and CO_2 gases which are subsequently influenced along their pathway through deep anoxic and very reducing conditions. This abiotic process is responsible for the N_2 reduction into NH_4^+ and CO_2 into CH_4 increasing NH_4^+ and CH_4 content in groundwater (Fig. 11). Then, still supplied by a local recharge, the water flows in contact with the organic material contained in the Miocene sediments. Biotic processes alter the sulfate isotopic and geochemical composition of those waters and increase the H_2S amount in surface waters (Type I) (Fig. 10 and 11).

Using this innovative and complex combination of tools, investigations highlight the occurrence of a regional gas supply observed in all thermo-mineral waters of the eastern part of Corsica Island, even in a non-tectonically active zone. The geological structural complexity of the island is responsible for a wide variety of processes affecting gas and water composition and explains the high diversity of thermo-mineral water observed, as shown in Fig. 10. The complexity and the diversity of processes accumulating along the regional path confirm the

involvement of gas and water mixing processes between the different geological units. To achieve a more sustainable use of thermo-mineral springs on the island of Corsica, quantifying the interplay between regional and local flows must be considered for future research. Indeed, due to the complexity of the flow paths involving, deep upwelling, interactions with the local geological matrix and mixing with phreatic waters, quantification of mixing ratios will be helpful in a further attempt to contribute to a more sustainable exploitation of the island's thermo-mineral springs.

5. Conclusion

These investigations aimed to provide new information on the accumulation of hydrogeological processes along groundwater flow-paths within tectonically non-active zones. Our findings demonstrate that groundwater gas contents can provide an almost complete assessment of hydrogeological processes (abiotic and biotic) occurring on both regional and local scales. This approach reveals not easily discernible insights by using more conventional hydrogeochemical and isotopic tools.

The use of dissolved gases as tracers circumvents the methodological constraints often encountered with classic tools, due to the presence of CO_2, iron, or sulfur, which can constrain the water analyses. This unconventional method enables us to identify the flow paths irrespective of water type or encountered geological units making analysis possible independently of water intrinsic properties (conductivity, pH, carbon or sulfide content).

In conclusion, studying dissolved gas content is an unconventional yet valuable tool, providing qualitative information about aquifer hydrogeological functioning such as the recharge conditions, the regional flow paths, hydrogeological compartments mixing (deep versus phreatic) and the impact of bacterial activity on water composition.

However, it is important to acknowledge several limitations, which can be categorised into two: practical and technical aspects, as well as more generalised data interpretation. Practical and technical limitations include the need for careful sampling, rapid gas sample analysis (< 48H) and cautious transportation (avoiding sudden pressure changes). To respectively avoid, atmospheric contamination, gas consumption or production by biotic activity, or artificial degassing which could introduce results bias, especially for carbonaceous samples. The limitations of the methodology and data interpretation arise from the high diversity of dissolved gases measured in this study. Resulting in contrasting gas signatures that are easy to identify and differ significantly from the uncertainties associated with our analytical tools. Further studies are needed to evaluate the applicability and effectiveness of this methodology when applied to springs with lower geochemical and gas diversity.

To pave the way for further research, it remains to be seen whether the dissolved gas content can be used to mathematically quantify groundwater mixing along the flow path.Quantifying flow paths at the origin of mineral water genesis is imperative for the effective protection and management of exploited spa or bottled springs. Understanding processes involved in gases and water release is essential to ensure the sustainability and quality of these valuable resources. It would allow the identification of potential sources of contamination, monitor the influence of biotic factors, and assess the impact of external forces, such as climate change and anthropogenic activities. By quantifying flow paths, we gain insights into the hydrogeological dynamics that shape mineral water composition, enabling us to make informed decisions for resource preservation. This knowledge empowers stakeholders to safeguard the integrity of spa and bottled springs, ensuring their long-term availability and benefit to society. This significance is heightened when considering that currently remote regions in Europe, such as those hosting UNESCO World Heritage sites, have their economies dependent solely on the spa tourism and social appeal of these historically renowned mineral springs since the 18th century.

DECLARATION OF COMPETING INTEREST

The authors declare that they have no known competing financial interests or personal relationships that could have appeared to influence the work reported in this paper.

ACKNOWLEDGEMENT

This research was supported by the *Culletivittà di Corsica* through the GERHYCO interdisciplinary project dedicated to water management, ecology and hydro-ecosystem services in an island context.

DATA AVAILABILITY

Data will be made available on request.

685 List of Figures

724 by colour according to each type: CO_2, N_2 or CH_4 rich water.

725 Figure 10. Hydrogeological conceptual model of thermo-mineral waters from the eastern part of Corsica.
726 Established from gas composition in order to discriminate flow and processes involved along the
727 regional continuous flow path from mountains to plain.

728 Figure 11. Major gas-related processes according to each spring type. Type I : CH_4 & H_2S rich, Type II : N_2
729 rich and Type III : CO_2 rich. Oxi. Proc. : Oxidation process ; Red. Proc. : Reduction process.

730 List of tables

731 Table 1: Information about sites, spring localities, code name, type and altitude.

732 Table 2: Field parameters, hydrochemical and isotopic contents of thermo-mineral groundwaters.

733 Table 3: Concentration of dissolved gas sampled with analytical error. Helium and excess air calculation results.
734 (<LOD) limit of detection, (n.m) non-measured, (-) calculation not realisable due to high CO_2 degassing.

735 Table 4: CFC and SF_6 concentrations measured in water in pmol/L and pptv

736

REFERENCES

Aeschbach-Hertig, W., Peeters, F., Beyerle, U., Kipfer, R., 1999. Interpretation of dissolved atmospheric noble gases in natural waters. Water Resources Research 35, 2779–2792. https://doi.org/10.1029/1999WR900130.

Agnew, R.J., Halihan, T., 2018. Why Springs Bubble: A Framework for Gas Discharge in Groundwater. Groundwater 56: 859-870. https://doi.org/10.1111/gwat.12789.

Amaral, H.I.F., Midões, C., Kipfer, R., 2017. Helium evidences for mantle degassing in the groundwater of Madeira Island – Portugal. Applied Geochemistry 81, 98–108. https://doi.org/10.1016/j.apgeochem.2017.03.019.

Amaudric, D.C.S., 1973. Les relations entre Schistes lustres et Flyschs autochtones dans le Sud de la Corse alpine. Geologie Alpine 49, 5–12.

Angelone, M., Gasparini, C., Guerra, M., Lombardi, S., Pizzino, L., Quattrocchi, F., Sacchi, E., Zuppi, G.M., 2005. Fluid geochemistry of the Sardinian Rift-Campidano Graben (Sardinia, Italy): fault segmentation, seismic quiescence of geochemically "active" faults, and new constraints for selection of CO_2 storage sites. Applied Geochemistry 20, 317–340. https://doi.org/10.1016/j.apgeochem.2004.08.008.

Aquilina, L., and J.-R. De Dreuzy. 2011. 'Relationship of Present Saline Fluid with Paleomigration of Basinal Brines at the Basement/Sediment Interface (Southeast Basin – France)'. Applied Geochemistry 26 (12): 1933–45. https://doi.org/10.1016/j.apgeochem.2011.06.022.

Barros, R., Defourny, A., Collignon, A., Jobe, P., Dassargues, A., Piessens, K., Welkenhuysen, K., 2020. A review of the geology and origin of CO_2 in mineral water springs in east Belgium. Geol. Belg. https://doi.org/10.20341/gb.2020.023.

Benavente, O., Tassi, F., Reich, M., Aguilera, F., Capecchiacci, F., Gutiérrez, F., Vaselli, O., Rizzo, A., 2016. Chemical and isotopic features of cold and thermal fluids discharged in the Southern Volcanic Zone between 32.5°S and 36°S: Insights into the physical and chemical processes controlling fluid geochemistry in geothermal systems of Central Chile. Chemical Geology 420, 97–113. https://doi.org/10.1016/j.chemgeo.2015.11.010.

Berndt, M.E., Allen, D.E., Seyfried Jr, W.E., 1996. Reduction of CO_2 during serpentinization of olivine at 300 C and 500 bar. Geology 24, 351–354.

Berthier, F., Demange, J., Desplan, A., 1980. Etude préliminaire des ressources géothermiques de la Corse (Rapport final No. 80SGN784GTH). BRGM.

Beyerle, U., Aeschbach-Hertig, W., Hofer, M., Imboden, D.M., Baur, H., Kipfer, R., 1999. Infiltration of river water to a shallow aquifer investigated with 3H/3He, noble gases and CFCs. Journal of Hydrology 220, 169–185.

Bräuer, K., Kämpf, H., Niedermann, S., Wetzel, H.-U., 2017. Regional distribution pattern of carbon and helium isotopes from different volcanic fields in the French Massif Central: Evidence for active mantle degassing and water transport. Chemical Geology, Progress in the Application of Gas Geochemistry to Geothermal, Tectonic and Magmatic Studies 469, 4–18. https://doi.org/10.1016/j.chemgeo.2017.04.004.

Bruno, C., Dupré, G., Giorgetti, G., Giorgetti, J.P., Alesandri, J., 2001. Chi tempu face?: météorologie, climat et microclimats de la Corse., CRDP de Corse.

Busenberg, E., Plummer, L.N., 1992. Use of chlorofluorocarbons (CCl3F and CCl2F2) as hydrologic tracers and age-dating tools: The alluvium and terrace system of central Oklahoma. Water Resources Research 28, 2257–2283. https://doi.org/10.1029/92WR01263.

Caballero, Y., Lachassagne, P., Ladouche, B., 2006. Contribution à l'évaluation de la ressource en eau des aquifères de

socle des roches granitiques de Corse (Rapport final No. BRGM/RP-54541-FR).

Caritg, S., 2009a. Carte géologique harmonisée du département de la Corse du sud : Notice explicative (Rapport final No. brgm/rp-57749-FR). BRGM.

Caritg, S., 2009b. Carte géologique harmonisée du département de la haute-Corse : Notice explicative (Rapport final No. BRGM/RP-57748-FR). BRGM.

Cartwright, Ian, D. Cendón, M. Currell, and K. Meredith. 2017. 'A Review of Radioactive Isotopes and Other Residence Time Tracers in Understanding Groundwater Recharge: Possibilities, Challenges, and Limitations'. Journal of Hydrology 555 (December): 797–811. https://doi.org/10.1016/j.jhydrol.2017.10.053.

Casillas-Trasvina, A., B. Rogiers, K. Beerten, J. Pärn, L. Wouters, and K. Walraevens. 2022. 'Using Helium-4, Tritium, Carbon-14 and Other Hydrogeochemical Evidence to Evaluate the Groundwater Age Distribution: The Case of the Neogene Aquifer, Belgium'. Journal of Hydrology X 17:100132. https://doi.org/10.1016/j.hydroa.2022.100132.

Chambers, L.A., Gooddy, D.C., Binley, A.M., 2019. Use and application of CFC-11, CFC-12, CFC-113 and SF6 as environmental tracers of groundwater residence time: A review. Geoscience Frontiers 10, 1643–1652.

Chatton, E., Labasque, T., de La Bernardie, J., Guihéneuf, N., Bour, O., Aquilina, L., 2017. Field Continuous Measurement of Dissolved Gases with a CF-MIMS: Applications to the Physics and Biogeochemistry of Groundwater Flow. Environ. Sci. Technol. 51, 846–854. https://doi.org/10.1021/acs.est.6b03706.

Chelnokov, G.A., Bragin, I.V., Kharitonova, N.A., 2018. Geochemistry of mineral waters and associated gases of the Sakhalin Island (Far East of Russia). Journal of Hydrology 559, 942–953. https://doi.org/10.1016/j.jhydrol.2018.02.049.

Chiodini, G., Cardellini, C., Caliro, S., Avino, R., Donnini, M., Granieri, D., Morgantini, N., Sorrenti, D., Frondini, F., 2020. The hydrothermal system of Bagni San Filippo (Italy): fluids circulation and CO_2 degassing. Italian Journal of Geosciences 139, 383–397. https://doi.org/10.3301/IJG.2020.12.

Craw, D., Upton, P., Horton, T., Williams, J., 2013. Migration of hydrothermal systems in an evolving collisional orogen, New Zealand. Miner Deposita 48, 233–248. https://doi.org/10.1007/s00126-012-0421-8.

D'Amore, F., Fancelli, R., Caboi, R., 1987. Observations on the application of chemical geothermometers to some hydrothermal systems in Sardinia. Geothermics 16, 271–282. https://doi.org/10.1016/0375-6505(87)90006-X.

Darling, W. G., D. C. Gooddy, A. M. MacDonald, and B. L. Morris. 2012. 'The Practicalities of Using CFCs and SF6 for Groundwater Dating and Tracing'. Applied Geochemistry, 13th International Symposium on Water-Rock Interaction (WRI -13), 27 (9): 1688–97. https://doi.org/10.1016/j.apgeochem.2012.02.005.

Dewandel, B., Lachassagne, P., Zaidi, F.K., Chandra, S., 2011. A conceptual hydrodynamic model of a geological discontinuity in hard rock aquifers: Example of a quartz reef in granitic terrain in South India. Journal of Hydrology 405, 474–487. https://doi.org/10.1016/j.jhydrol.2011.05.050.

Di Rosa, M., De Giorgi, A., Marroni, M., Vidal, O., 2017. Syn-convergence exhumation of continental crust: evidence from structural and metamorphic analysis of the Monte Cecu area, Alpine Corsica (Northern Corsica, France). Geological Journal 52, 919–937. https://doi.org/10.1002/gj.2857

Dominici, R., Iundt, F., Juncy, G., Mickaelly, B., 1986. Prospection des anomalies gazeuses liées a l'hydrothermalisme de Puzzichellu - commune d'Aghione (Haute Corse) (No. 86SGN002CSC), BRGM. Bastia.

Dupalová, T., Sracek, O., Vencelides, Z., Žák, K., 2012. The origin of thermal waters in the northeastern part of the Eger Rift, Czech Republic. Applied geochemistry 27, 689–702.

Dupuy, M., Garel, E., Huneau, F., Santoni, S., Di Rosa, M., Mattei, A., 2021. Geochemical and isotope characterisation of thermo-mineral springs of Corsica Island: from geological complexity to groundwater singularity. Water 13, 2413. https://doi.org/10.3390/w13172413.

Elena, F., Vasiliy, L., Natalia, K., Arslan, S., Elena, M., Ekaterina, B., Anna, K., Alexey, M., Elena, B., 2020. Hydrogeology and hydrogeochemistry of mineral sparkling groundwater within Essentuki area (Caucasian mineral water region). Environmental Earth Sciences 79, 1–12.

Epstein, Gabe S., Gray E. Bebout, B.W. Christenson, H. Sumino, I. Wada, C. Werner, and D.R. Hilton. 2021. 'Cycling of CO2 and N2 Along the Hikurangi Subduction Margin, New Zealand: An Integrated Geological, Theoretical, and Isotopic Approach'. Geochemistry, Geophysics, Geosystems 22 (9): e2021GC009650. https://doi.org/10.1029/2021GC009650.

Etiope, G., 2017. Abiotic Methane in Continental Serpentinization Sites: An Overview. Procedia Earth and Planetary Science, 15th Water-Rock Interaction International Symposium, WRI-15 17, 9–12. https://doi.org/10.1016/j.proeps.2016.12.006.

Everitt, B.S., Dunn, G., 2001. Principal Components Analysis, in: Applied Multivariate Data Analysis. John Wiley & Sons, Ltd, pp. 48–73. https://doi.org/10.1002/9781118887486.ch3

Faramawy, S., Zaki, T., Sakr, A.A.-E., 2016. Natural gas origin, composition, and processing: A review. Journal of Natural Gas Science and Engineering 34, 34–54. https://doi.org/10.1016/j.jngse.2016.06.030

Genevier, M., Mardhel, V., Frissant, N., 2011. Actualisation de la synthèse hydrogéologique de la région Corse (Rapport final No. BRGM/RP-59924-FR). BRGM.

Giggenbach, W.F., 1991. Chemical techniques in geothermal exploration. Application of geochemistry in geothermal reservoir development 119–144.

Giggenbach, W.F., 1988. Geothermal solute equilibria. Derivation of Na-K-Mg-Ca geoindicators. Geochimica et Cosmochimica Acta 52, 2749–2765. https://doi.org/10.1016/0016-7037(88)90143-3.

Giggenbach, W.F., Gonfiantini, R., Jangi, B.L., Truesdell, A.H., 1983. Isotopic and chemical composition of parbati valley geothermal discharges, North-West Himalaya, India. Geothermics 12, 199–222. https://doi.org/10.1016/0375-6505(83)90030-5.

Gilhooly, W.P., Fike, D.A., Druschel, G.K., Kafantaris, F.-C.A., Price, R.E., Amend, J.P., 2014. Sulfur and oxygen isotope insights into sulfur cycling in shallow-sea hydrothermal vents, Milos, Greece. Geochem Trans 15, 12. https://doi.org/10.1186/s12932-014-0012-y.

Goswami, S., AK. Rai, and S. Tripathy. 2022. 'Re-Visiting Geothermal Fluid Circulation, Reservoir Depth and Temperature of Geothermal Springs of India'. Journal of Hydrology 612 (September): 128131. https://doi.org/10.1016/j.jhydrol.2022.128131.

Grasby, S.E., Hutcheon, I., Krouse, H.R., 2000. The influence of water–rock interaction on the chemistry of thermal springs in western Canada. Applied Geochemistry 15, 439–454. https://doi.org/10.1016/S0883-2927(99)00066-9.

Gueydan, F., Brun, J.-P., Phillippon, M., Noury, M., 2017. Sequential extension as a record of Corsica Rotation during Apennines slab roll-back. Tectonophysics, Evolution of fore-arc and back-arc sedimentary basins with focus on the Japan subduction system and its analogues 710–711, 149–161. https://doi.org/10.1016/j.tecto.2016.12.028.

Hiscock, K.M., 2009. Hydrogeology: principles and practice. John Wiley & Sons.

Jenden, P.D., Titley, P.A., Worden, R.H., 2015. Enrichment of nitrogen and 13C of methane in natural gases from the Khuff Formation, Saudi Arabia, caused by thermochemical sulfate reduction. Organic Geochemistry 82, 54–68.

Juhlke, T.R., Sültenfuß, J., Trachte, K., Huneau, F., Garel, E., Santoni, S., Barth, J.A., Geldern, R. van, 2020. Tritium as a hydrological tracer in Mediterranean precipitation events. Atmospheric Chemistry and Physics 20, 3555–3568.

Karolytė, R., Johnson, G., Györe, D., Serno, S., Flude, S., Stuart, F.M., Chivas, A.R., Boyce, A., Gilfillan, S.M.V., 2019. Tracing the migration of mantle in gas fields and mineral water springs in south-east Australia using noble gas and stable isotopes. Geochimica et Cosmochimica Acta 259, 109–128. https://doi.org/10.1016/j.gca.2019.06.002.

Karolytė, R., Serno, S., Johnson, G., Gilfillan, S.M.V., 2017. The influence of oxygen isotope exchange between CO 2 and H 2 O in natural CO 2 -rich spring waters: Implications for geothermometry. Applied Geochemistry 84, 173–186. https://doi.org/10.1016/j.apgeochem.2017.06.012.

Kim, K.-H., Yun, S.-T., Yu, S., Choi, B.-Y., Kim, M.-J., Lee, K.-J., 2020. Geochemical pattern recognitions of deep thermal groundwater in South Korea using self-organizing map: Identified pathways of geochemical reaction and mixing. Journal of Hydrology 589, 125202. https://doi.org/10.1016/j.jhydrol.2020.125202

Kipfer, R., Aeschbach-Hertig, W., Peeters, F., Stute, M., 2002. Noble gases in lakes and ground waters. Reviews in mineralogy and geochemistry 47, 615–700.

Kotowski, T., L. Chudzik, and J. Najman. 2019. 'Application of Dissolved Gases Concentration Measurements, Hydrochemical and Isotopic Data to Determine the Circulation Conditions and Age of Groundwater in the Central Sudetes Mts'. Journal of Hydrology 569 (February): 735–52. https://doi.org/10.1016/j.jhydrol.2018.12.013.

Kulongoski, Justin T., David R. Hilton, Richard G. Cresswell, Stephen Hostetler, and Gerry Jacobson. 2008. 'Helium-4 Characteristics of Groundwaters from Central Australia: Comparative Chronology with Chlorine-36 and Carbon-14 Dating Techniques'. Journal of Hydrology 348 (1): 176–94. https://doi.org/10.1016/j.jhydrol.2007.09.048.

Lachassagne, P., 2011. The fracture permeability of Hard Rock Aquifers is due neither to tectonics, nor to unloading, but to weathering processes. Terra Nova 145–161. https://doi.org/10.1111/j.1365-3121.2011.00998.x.

Lavrushin, V.Y., Israfailov, Y.G., Polyak, B.G., Pokrovsky, B.G., Bujakaite, M.I., Kamensky, I.L., 2018. Conditions of the formation of thermomineral waters in the Talysh fold zone of the Lesser Caucasus (Azerbaijan) based on isotope-geochemical data (3He/4He, δ13C co2, δ13Cch4, δ15N-N2, 87Sr/86Sr, δD-H2O, and δ18O-H2O). Lithology and Mineral Resources 53, 53–75. https://doi.org/10.1134/S0024490217060050.

Lee, J.M., Koh, D.-C., Chae, G.-T., Kee, W.-S., Ko, K.-S., 2021. Integrated assessment of major element geochemistry and geological setting of traditional natural mineral water sources in South Korea at the national scale. Journal of Hydrology 598, 126249. https://doi.org/10.1016/j.jhydrol.2021.126249.

Loÿe-Pilot, M.-D., Durand-Delga, M., Feinberg, H., Gourinard, Y., Magné, J., 2004. Les formations burdigaliennes de Corse orientale dans leur cadre géodynamique. Comptes Rendus Geoscience 336, 919–930. https://doi.org/10.1016/j.crte.2004.02.011.

Machel, H.G., 2001. Bacterial and thermochemical sulfate reduction in diagenetic settings Ð old and new insights. Sedimentary Geology 33.

Malvoisin, B., Chopin, C., Brunet, F., Galvez, M.E., 2012. Low-temperature Wollastonite Formed by Carbonate Reduction: a Marker of Serpentinite Redox Conditions. Journal of Petrology 53, 159–176. https://doi.org/10.1093/petrology/egr060.

Marques, J.M., Eggenkamp, H.G.M., Carreira, P.M., Antunes da Silva, M., 2020. Origin and evolution of Cl in CO2-rich

thermal and mineral waters from northern Portugal. Applied Geochemistry 116, 104569. https://doi.org/10.1016/j.apgeochem.2020.104569.

Marques, J.M., Etiope, G., Neves, M.O., Carreira, P.M., Rocha, C., Vance, S.D., Christensen, L., Miller, A.Z., Suzuki, S., 2018. Linking serpentinization, hyperalkaline mineral waters and abiotic methane production in continental peridotites: an integrated hydrogeological-bio-geochemical model from the Cabeço de Vide CH4-rich aquifer (Portugal). Applied Geochemistry 96, 287–301. https://doi.org/10.1016/j.apgeochem.2018.07.011.

Marques, J.M., Carreira, P.M.M., Aires-Barros, L., Graça, R.C., 2000. Nature and role of CO2 in some hot and cold HCO 3 /Na/CO 2 -rich Portuguese mineral waters: a review and reinterpretation. Environmental Geology 40, 53–63. https://doi.org/10.1007/s002540000151.

Martín-Loeches, M., Pavón-García, J., Molina-Navarro, E., Martínez-Santos, P., Almeida, C., Reyes-López, J., Cienfuegos-Hevia, I., Sastre-Merlín, A., 2020. Hydrogeochemistry of granitic mountain zones and the influence of adjacent sedimentary basins at their tectonic borders: the case of the Spanish Central System batholith. Hydrogeol J. https://doi.org/10.1007/s10040-020-02202-1.

Mattei, A., Huneau, F., Garel, E., Santoni, S., Vystavna, Y., 2021. Evaporation in Mediterranean conditions: estimations based on isotopic approaches at the watershed scale. Hydrological Processes n/a. https://doi.org/10.1002/hyp.14085

Michard, G., 1990. Behaviour of major elements and some trace elements (Li, Rb, Cs, Sr, Fe, Mn, W, F) in deep hot waters from granitic areas. Chemical Geology 89, 117–134.

Mikhail, S., Sverjensky, D.A., 2014. Nitrogen speciation in upper mantle fluids and the origin of Earth's nitrogen-rich atmosphere. Nature Geoscience 7, 816–819. https://doi.org/10.1038/ngeo2271.

Minissale, A., 2004. Origin, transport and discharge of CO_2 in central Italy. Earth-Science Reviews 66, 89–141. https://doi.org/10.1016/j.earscirev.2003.09.001.

Minissale, A., Donato, A., Procesi, M., Pizzino, L., Giammanco, S., 2019. Systematic review of geochemical data from thermal springs, gas vents and fumaroles of Southern Italy for geothermal favourability mapping. Earth-Science Reviews 188, 514–535. https://doi.org/10.1016/j.earscirev.2018.09.008.

Minissale, A., Magro, G., Martinelli, G., Vaselli, O., Tassi, G.F., 2000. Fluid geochemical transect in the Northern Apennines (central-northern Italy): fluid genesis and migration and tectonic implications. Tectonophysics 319, 199–222. https://doi.org/10.1016/S0040-1951(00)00031-7.

Minissale, A., Magro, G., Tassi, F., Frau, F., Vaselli, O., 1999. The origin of natural gas emissions from Sardinia island, Italy. Geochemical journal 33, 1–12.

Moritz, A., Hélie, J.-F., Pinti, D.L., Larocque, M., Barnetche, D., Retailleau, S., Lefebvre, R., Gélinas, Y., 2015. Methane Baseline Concentrations and Sources in Shallow Aquifers from the Shale Gas-Prone Region of the St. Lawrence Lowlands (Quebec, Canada). Environ. Sci. Technol. 49, 4765–4771. https://doi.org/10.1021/acs.est.5b00443.

Mörner, N.-A., Etiope, G., 2002. Carbon degassing from the lithosphere. Global and Planetary Change 33, 185–203.

Nlend, B., Huneau, F., Garel, E., Santoni, S., Mattei, A., 2023. Precipitation isoscapes in areas with complex topography: Influence of large-scale atmospheric dynamics versus microclimatic phenomena. Journal of Hydrology 617, 128896. https://doi.org/10.1016/j.jhydrol.2022.128896.

Paternoster, M., Oggiano, G., Sinisi, R., Caracausi, A., Mongelli, G., 2017. Geochemistry of two contrasting deep fluids in the Sardinia microplate (western Mediterranean): Relationships with tectonics and heat sources. Journal of Volcanology and Geothermal Research 336, 108–117. https://doi.org/10.1016/j.jvolgeores.2017.02.011.

Paull, C., Lorenson, T., Borowski, W., Ussler, B., Olsen, K., Rodriguez, N., 2000. Isotopic composition of CH_4, CO_2 species, and sedimentary organic matter within samples from the Blake Ridge: Gas source implications. Proceedings of the Ocean Drilling Program: Scientific Results 164. https://doi.org/10.2973/odp.proc.sr.164.207.2000.

Penna, D., Stenni, B., Šanda, M., Wrede, S., Bogaard, T. A., Gobbi, A., Borga, M., Fischer, B. M. C., Bonazza, M., and Chárová, Z., 2010. On the reproducibility and repeatability of laser absorption spectroscopy measurements for δ2H and δ18O isotopic analysis, Hydrol. Earth Syst. Sci., 14, 1551–1566, https://doi.org/10.5194/hess-14-1551-2010.

Petrović, T., Zlokolica-Mandić, M., Veljković, N., Vidojević, D., 2010. Hydrogeological conditions for the forming and quality of mineral waters in Serbia. Journal of Geochemical Exploration 107, 373–381.

Piccoli, F., Vitale Brovarone, A., Ague, J.J., 2018. Field and petrological study of metasomatism and high-pressure carbonation from lawsonite eclogite-facies terrains, Alpine Corsica. Lithos 304–307, 16–37. https://doi.org/10.1016/j.lithos.2018.01.026.

Powell, T., Cumming, W., 2010. Spreadsheets for geothermal water and gas geochemistry, in: Proceedings. pp. 1–3.

Ravna, E.J.K., Andersen, T.B., Jolivet, L., Capitani, C.D., 2010. Cold subduction and the formation of lawsonite eclogite – constraints from prograde evolution of eclogitized pillow lava from Corsica. Journal of Metamorphic Geology 28, 381–395. https://doi.org/10.1111/j.1525-1314.2010.00870.x.

Rojey, A., 1997. Technological innovations in gas field operations; L'innovation technique dans l'exploitation des ressources gazieres. Gaz d'Aujourd'hui (Paris), 121 : 404-407, ISSN : 0016-5328.

Rome, S., Giorgetti, J.-P., 2007. Corsican mountains and its climatic features [WWW Document]. URL https://doi.org/10.4267/2042/14846.

Rossi, P., Cocherie, A., Fanning, C.M., 2015. Evidence in Variscan Corsica of a brief and voluminous Late Carboniferous to Early Permian volcanic-plutonic event contemporaneous with a high-temperature/low-pressure metamorphic peak in the lower crust. Bulletin de la Société Géologique de France 186, 171–192.

Ruzié, L., Aubaud, C., Moreira, M., Agrinier, P., Dessert, C., Gréau, C., Crispi, O., 2013. Carbon and helium isotopes in thermal springs of La Soufrière volcano (Guadeloupe, Lesser Antilles): implications for volcanological monitoring. Chemical Geology 359, 70–80.

Sacchi, E., Cuoco, E., Oster, H., Paolucci, V., Tedesco, D., Viaroli, S., 2022. Tracing groundwater circulation in a valuable mineral water basin with geochemical and isotopic tools: the case of FERRARELLE, Riardo basin, Southern Italy. Environ Geochem Health 44, 1–28. https://doi.org/10.1007/s10653-021-00845-x.

Serrano, O., Allanic, C., Magar, M., 2013. Synthèse géologique du bassin tertiaire de la Plaine orientale Corse - Liaison Terre-Mer entre San Nicolao et Solenzara (Rapport final No. BRGM/RP-62303-FR).

Sherwood Lollar, B., Westgate, T.D., Ward, J.A., Slater, G.F., Lacrampe-Couloume, G., 2002. Abiogenic formation of alkanes in the Earth's crust as a minor source for global hydrocarbon reservoirs. Nature 416, 522–524. https://doi.org/10.1038/416522a.

Štrbački, J., Živanović, V., Ćuk Đurović, M., Atanacković, N., Dragišić, V., 2020. Origin, diversity and geothermal potentiality of thermal and mineral waters in Vrnjačka Banja, Serbia. Environ Earth Sci 79, 309. https://doi.org/10.1007/s12665-020-09050-y.

Tarvainen, T., Sapon, S., Jarva, J., 2019. Applying heatmaps in interpretation of geochemical baseline data on urban soils in Finland. Journal of Geochemical Exploration 205, 106345. https://doi.org/10.1016/j.gexplo.2019.106345

967 Tassi, F., Feyzullayev, A.A., Bonini, M., Sani, F., Aliyev, C.S., Darrah, T.H., Vaselli, O., Baghirli, R.J., 2020. Mantle vs.
968 crustal fluid sources in the gas discharges from Lesser Caucasus and Talysh Mountains (Azerbaijan) in relation to
969 the regional geotectonic setting. Applied Geochemistry 118, 104643.
970 https://doi.org/10.1016/j.apgeochem.2020.104643.

971 Thatcher, L.L., Janzer, V.J., Edwards, K.W., 1977. Methods for Determination of Radioactive Substances in Water and
972 Fluvial Sediments. U.S. Government Printing Office.

973 Thiébaud, E., Dzikowski, M., Gasquet, D., Renac, C., 2010. Reconstruction of groundwater flows and chemical water
974 evolution in an amagmatic hydrothermal system (La Léchère, French Alps). Journal of Hydrology 381, 189–202.
975 https://doi.org/10.1016/j.jhydrol.2009.11.041.

976 Vitale Brovarone, A., Beyssac, O., Malavieille, J., Molli, G., Beltrando, M., Compagnoni, R., 2013. Stacking and
977 metamorphism of continuous segments of subducted lithosphere in a high-pressure wedge: The example of Alpine
978 Corsica (France). Earth-Science Reviews 116, 35–56. https://doi.org/10.1016/j.earscirev.2012.10.003

979 Werner, C., C. I. Schipper, S. J. Cronin, P. H. Barry, and M. K. Stewart. 2022. 'Magmatic Carbon and Helium in Springs
980 Reveals the Vitality of a Dormant Volcano, Taranaki, New Zealand'. Geophysical Research Letters 49 (18):
981 e2022GL099273. https://doi.org/10.1029/2022GL099273.

982 Whiticar, M.J., Faber, E., Schoell, M., 1986. Biogenic methane formation in marine and freshwater environments: CO_2
983 reduction vs. acetate fermentation—Isotope evidence. Geochimica et Cosmochimica Acta 50, 693–709.
984 https://doi.org/10.1016/0016-7037(86)90346-7.

985 Zippa, E., Plyusnin, A., Shvartsev, S., 2019. The chemical and isotopic compositions of thermal waters and gases in the
986 Republic of Buryatia, Russia. E3S Web Conf. 98, 01055. https://doi.org/10.1051/e3sconf/20199801055.

Tables

Table 1: Information about sites, springs localities, code name, type and altitude.

Spring name	CODE	Type	Geographic Coordinates			
			Altitude (m asl)	in " Lambert 93"		Municipality
				X (m)	Y (m)	
Acqua Acetosa	ACQ	Spring	47	1,227,704.289	6,119,785.550	*Serra di Fiumorbo*
Caldaniccia Travu	CALD	Spring	284	1,220,620.598	6,111,725.565	*Chisa*
Vignola Travu	VIGN	Spring	190	1,223,000.993	6,112,347.655	*Chisa*
Fontanella	FONT	Spring	1	1,231,781.421	6,107,000.355	*Solaro*
Pietrapola	P-MUR3	Spring	190	1,222,833.837	6,119,744.012	*Isolaccio-di-Fiumorbo*
	P-LAV	Spring				
	P-LEC	Spring				
	P-LUC	Spring				
	P-MUR1	Spring				
	P-ESC	Spring				
	P-RAST	Spring				

	P-SOA	Spring				
Campo-Favajo	CAM-F	Spring	25	1,231,884.619	6,137,973.405	*Antisanti*
Puzzichellu	PUZ-F	Borehole	60	1,230,383.109	6,135,227.581	*Aghione*
	PUZ-N	Spring				
	PUZ-G	Spring				
Fajo-Quarcio	QUAR-D	Spring	110	1,228,744.504	6,142,058.466	*Giuncaggio*
	QUAR-G	Spring	110			
Vadina	VAD	Spring	18	1,234,334.584	6,129,574.738	*Ghisonaccia*
Pardina	PARD	Spring	554	1,228,492.188	6,158,708.617	*Tarrano*
Moïta	MOIT	Spring	442	1,228,931.829	6,152,106.468	*Moïta*
Forcione	FORC	Spring	177	1,227,838.685	6,169,146.731	*Scata*
La Porta	PORT	Spring	369	1,223,782.856	6,169,454.126	*Poggio Marinaccio*
Piana	PIAN	Spring	370	1,225,496.502	6,164,172.761	*Stazzona*
Surgente Sottana	SSOT	Borehole	415	1,225,544.676	6,163,060.865	*Rappaggio*

Surgente Supprana	SSUP	Spring	477	1,225,594.739	6,163,049.761	*Rappaggio*
Caldane d'Ampugnani	AMPU	Spring	159	1,229,540.988	6,168,923.534	*San Gavino d'Ampugnani*

Table 2: Field parameters, hydrochemical and isotopic content of thermo-mineral groundwaters.

SPRINGS CODE	DATE	T.	pH	E.C.	Eh	O_2		HCO_3^-	CO_3^{2-}	NH_4	3H		^2H		^{18}O		Estimated recharge altitude (m.a.s.l.)	
		°C	-	µS/cm²	mV	mg/L	%	mg/L	mg/L	mg/L	TU	*STD*	‰	*STD*	‰	*STD*	*Ave.*	*STD*
ACQ	Apr-18	15.7	5.93	2150	310	0.85	8.7	1437	1.3E-03	0.27			-40.03	0.10	-7.22	0.03	263	34
	Dec-18	17.9	6.01	2120	228	0.28	2.9	1291	1.4E-03	0.08	1.1	0.2	-38.69	0.38	-6.88	0.00		
AMPU	Apr-18	13.5	5.99	1126	319	3.85	37.9	798	8.3E-04				-43.52	0.09	-7.63	0.05	458	32
	Sep-18	15.7	5.96	1432	338	2.49	25.1	937	9.1E-04	2.17	1.7	0.2	-44.56	0.14	-8.08	0.06		
	Dec-18	12.9	5.83	1237	356	3.40	32.8	836	6.0E-04	1.63			-43.04	0.34	-7.86	0.03		
CALD	Apr-18	33	9.58	150	2	2.11	0.3	63	2.6E-01	1.59			-52.11	0.07	-8.17	0.02	1035	115
CAM-F	Apr-18	16.5	7.83	1405	196	0.25	2.5	468	3.4E-02				-39.64	0.27	-7.13	0.04	228	17
	Sep-18	17.1	7.78	1429	-90	0.01	0.1	494	3.2E-02		0.0		-39.21	0.24	-7.05	0.05		
	Dec-18	16.6	7.67	1381	-111	0.16	1.6	461	2.3E-02				-39.05	0.10	-6.83	0.16		
FAJO-D	Apr-18	15.7	7.35	698	-25	25.00	2.45	503	1.3E-02				-41.18	0.18	-7.44	0.02	292	35

	Sep-18	16.8	7.03	693	67	-	-	538	6.1E-03		1.3	0.2	-41.30	0.50	-7.37	0.03		
	Dec-18	16.2	7.11	700	-4	2.34	22.9	405	5.5E-03				-39.79	0.34	-7.19	0.09		
	Apr-18	15.5	7.30	704	-34	28.60	2.81	438	9.3E-03				-40.69	0.56	-7.26	0.04		
FAJO-G	Sep-18	16.7	7.16	694	39	-	-	400	6.2E-03		1.1	0.2	-41.19	0.69	-7.51	0.12	277	25
	Dec-18	16.3	7.02	711	9	1.90	19.5	372	4.1E-03				-39.98	0.14	-7.23	0.07		
	Apr-18	17.5	6.13	12150	190	0.02	0.2	1696	2.4E-03				-41.30	0.47	-7.39	0.04		
FONT	Sep-18	19.5	6.06	12200	222	0.20	2	1764	2.2E-03		1.2	0.2	-42.70	0.55	-7.07	0.03	334	45
	Dec-18	18.9	6.46	12070	178	0.77	8.1	1787	5.5E-03				-41.01	0.12	-6.94	0.02		
	Apr-18	15.2	5.77	1002	275	0.08	0.8	676	4.3E-04				-46.08	0.31	-7.91	0.12		
FORC	Sep-18	15.4	5.79	1026	290	0.75	7.6	665	4.4E-04		0.0		-46.66	0.07	-8.23	0.07	580	17
	Dec-18	15.4	5.80	1022	298	0.17	1.7	689	4.6E-04				-46.03	0.10	-8.23	0.10		
	Apr-18	13.5	5.99	1149	311	0.70	7	781	8.1E-04				-47.40	0.44	-8.37	0.01		
MOIT																	650	24
	Sep-18	14.9	5.89	1216	279	-	-	856	7.1E-04	0.24	0.0		-47.05	0.34	-8.15	0.04		

	Dec-18	13.8	5.99	1010	279	0.52	5.3	694	7.2E-04	0.25			-46.81	0.58	-8.16	0.08		
PARD	Apr-18	12	5.44	516	402	1.52	15.3	265	7.8E-05	0.17			-48.36	0.31	-8.50	0.06		
	Sep-18	12.5	5.53	556	233	0.55	5.6	314	1.1E-04	0.06	2.3	0.3	-48.57	0.40	-8.40	0.02	702	41
	Dec-18	12.1	5.20	497	373	1.61	16	275	4.7E-05	0.01			-47.84	0.40	-8.28	0.02		
P-B	Sep-18	44	8.89	372	-185	0.54		128	1.1E-01		0.0		-54.81	0.30	-9.22	0.06		
	Dec-18	43.2	9.67	338	-61	4.04	67.1	100	5.0E-01				-55.06	0.20	-9.10	0.04	1045	17
P-LAV	Apr-18	48.6	9.18	336	189	0.53	9.8	122	1.9E-01				-54.65	0.22	-9.09	0.05		
	Sep-18	48.9	9.00	376	-174	2.43		118	1.3E-01		0.0		-54.47	0.03	-8.96	0.02	1045	21
	Dec-18	49.9	9.63	340	-123	0.55	9.8	110	4.9E-01	0.56			-55.26	0.28	-9.35	0.07		
P-LUC	Apr-18	31.3	9.32	334	202	3.89	48.4	110	2.4E-01	0.46			-54.96	0.24	-9.33	0.05		
	Sep-18	34.5	9.36	338	19	1.42	20.4	132	3.2E-01	0.32	0.0		-51.63	0.13	-8.62	0.06	1031	43
	Dec-18	32.5	9.60	336	-82	1.17	16.5	109	4.6E-01	0.43			-54.97	0.16	-8.85	0.06		
P-MUR3	Dec-18	50.1	9.38	338	-98	2.06	37.1	112	1.8E-01	0.47			-54.10	0.31	-8.89	0.08	1036	24

	Sep-18	49.7	8.96	378	-182	-	-	116	1.1E-01		0.0		-55.58	0.03	-9.09	0.00		
	Apr-18	49	9.15	337	189	2.33	42.6	118	2.9E-01				-55.20	0.23	-9.17	0.03		
PORT	Apr-18	12.1	6.17	2390	259	1.14	11	1642	2.6E-03				-54.29	0.36	-9.03	0.12	1061	26
	Sep-18	15.9	5.98	3140	110	0.24	2.6	2102	2.1E-03		0.0		-54.83	0.08	-9.20	0.06		
P-RAST	Sep-18	54.7	8.96	340	-24	0.99	18.1	105	1.0E-01		0.0		-55.19	0.03	-9.21	0.04	1043	17
	Dec-18	54.2	9.20	340	-147	1.22	22.7	121	2.0E-01				-54.67	0.13	-9.05	0.03		
P-SOA	Apr-18	50.7	9.09	339	188	0.65	11.6	131	1.7E-01				-55.02	0.55	-9.18	0.01		
	Sep-18	50.8	9.16	375	-170	0.06	1.1	133	2.0E-01	1.41	0.0		-54.71	0.49	-9.03	0.07	1047	20
	Dec-18	49.4	9.55	340	-175	0.82	14.5	106	4.0E-01	1.39			-54.68	0.38	-8.79	0.08		
PUZ-F	Apr-18	16.7	7.32	1800	213	6.30	63.4	559	1.2E-02				-38.65	0.59	-6.70	0.05		
	Sep-18	16.9	7.10	1048	18	0.12	1.2	498	6.6E-03		1.3	0.2	-38.55	0.26	-7.07	0.06	199	14
	Dec-18	16.7	7.17	1052	-125	0.24	2.5	492	7.8E-03				-38.28	0.21	-6.92	0.04		
PUZ-N	Apr-18	14.2	6.96	1309	214	1.60	16.2	559	5.4E-03	0.25			-38.13	0.31	-6.81	0.03	163	29

	Sep-18	17.5	7.05	1592	-107	1.14	11.4	616	7.4E-03	0.29	0.0		-38.81	0.81	-7.18	0.07		
	Dec-18	15.5	6.96	1325	-119	1.49	14.9	577	5.6E-03	0.12			-38.00	0.30	-6.88	0.03		
	Apr-18	13.6	5.69	920	302	0.91	9.3	659	3.5E-04	0.11			-49.02	0.45	-8.50	0.09		
S-SOT	Sep-18	13.7	5.72	910	308	0.62	6.2	580	3.2E-04	0.09	1.8	0.2	-50.28	0.22	-8.43	0.05	753	29
	Dec-18	13.7	5.72	962	309	1.09	11.1	628	3.5E-04				-49.06	0.30	-8.43	0.09		
	Apr-18	11.7	4.96	254	281	0.75	0.7	115	1.1E-05				-49.60	0.07	-8.61	0.06		
S-SUP	Sep-18	12.5	4.96	257	272	0.02	0.2	83	8.1E-06		1.2	0.2	-49.61	0.15	-8.48	0.03	780	20
	Dec-18	12.2	4.88	255	217	0.01	0.1	98	7.9E-06				-50.01	0.13	-8.54	0.07		
	Apr-18	27.7	7.51	2.89	0	2.63	34	67	2.3E-03	0.34			-55.19	0.18	-9.38	0.05		
VIGN	Sep-18	28.7	8.03	2880	49	2.00	26.1	29	3.3E-03	1.56			-51.63	0.19	-8.77	0.11	876	103
	Dec-18	28	7.47	2870	-20	2.57	33.5	110	3.4E-03				-52.00	0.32	-8.80	0.07		

Table 3: Concentration of dissolved gas sampled with analytical error. Helium and excess air calculation results. (<LOD) limit of detection, (n.m) non-measured, (-) calculation not allowed due to high CO_2 degassing.

SPRING CODE	DATE	CO_2	He	Ne	H_2	Ar	O_2	N_2	CH_4	H_2S	N_2/Ar	He excess	Excess Air
		± 5%	± 3%	± 3%	± 3%	± 3%	± 3%	± 5%	± 3%	± 3%			(EA)
		mol/L										cm^3STP/g	
ACQ	Apr-18	2.94E-02	5.90E-09	1.79E-09	<LOD	3.42E-06	8.84E-07	1.16E-04	6.38E-07	<LOD	34	-	-
ACQ	Dec-18	3.60E-02	n.m	8.89E-10	<LOD	4.59E-07	1.44E-06	3.84E-05	2.49E-07	<LOD	84	-	-
S-SOT	Apr-18	5.61E-02	3.69E-09	1.17E-09	<LOD	5.24E-06	3.75E-07	1.85E-04	5.33E-07	3.03E-07	35	-	-
S-SOT	Sept-18	3.59E-02	n.m	2.71E-09	<LOD	4.91E-06	5.63E-07	1.95E-04	5.96E-07	<LOD	40	-	-
S-SOT	Dec-18	3.89E-02	n.m	<LOD	<LOD	2.08E-06	1.34E-07	7.24E-05	3.10E-07	5.17E-07	35	-	-
S-SUP	Apr-18	5.00E-02	2.76E-10	<LOD	<LOD	1.64E-06	2.27E-07	5.50E-05	2.18E-08	<LOD	33	-	-
S-SUP	Sept-18	2.30E-02	n.m	<LOD	<LOD	3.66E-07	3.18E-07	2.52E-05	0.00E+00	5.65E-07	69	-	-
S-SUP	Dec-18	3.14E-02	n.m	8.16E-10	<LOD	1.08E-06	2.41E-07	4.05E-05	9.10E-08	1.03E-06	38	-	-
AMPU	Apr-18	2.51E-02	3.37E-09	5.47E-09	<LOD	8.40E-06	1.06E-04	2.78E-04	4.76E-08	<LOD	33	-	-
AMPU	Sept-18	1.79E-02	n.m	1.10E-09	<LOD	1.96E-06	3.36E-06	7.82E-05	2.67E-08	<LOD	40	-	-

AMPU	Dec-18	1.99E-02	1.05E-09	3.49E-09	<LOD	7.96E-06	9.51E-05	2.95E-04	3.61E-08	<LOD	37	-	-
FONT	Apr-18	3.37E-02	1.35E-09	1.37E-09	<LOD	1.25E-06	1.10E-07	4.20E-05	9.29E-07	6.77E-08	34	-	-
FONT	Dec-18	2.28E-02	n.m	<LOD	<LOD	3.22E-07	1.92E-07	1.10E-05	3.79E-07	<LOD	34	-	-
FONT	Sept-18	1.95E-02	n.m	3.13E-10	1.84E-08	5.77E-07	1.09E-06	2.20E-05	5.32E-07	<LOD	38	-	-
FORC	Apr-18	3.09E-02	1.26E-08	1.68E-09	<LOD	1.05E-05	1.35E-07	4.17E-04	1.04E-06	<LOD	40	-	-
FORC	Sept-18	1.93E-02	n.m	2.34E-09	<LOD	6.72E-06	4.13E-07	3.01E-04	8.27E-07	<LOD	45	-	-
FORC	Dec-18	2.49E-02	1.89E-08	3.20E-09	<LOD	9.08E-06	4.60E-07	4.23E-04	1.20E-06	6.77E-08	47	-	-
PORT	Apr-18	4.64E-02	n.m	<LOD	<LOD	2.83E-06	2.13E-07	9.52E-05	1.17E-05	<LOD	34	-	-
PORT	Sept-18	3.06E-02	n.m	<LOD	<LOD	8.02E-07	2.81E-06	2.80E-05	5.14E-06	<LOD	35	-	-
PARD	Apr-18	4.45E-02	4.15E-09	2.56E-09	<LOD	3.46E-06	1.82E-05	1.10E-04	1.74E-07	<LOD	32	-	-
CALD	Apr-18	3.50E-06	2.53E-08	7.93E-09	<LOD	1.72E-05	1.24E-05	5.85E-04	2.38E-07	<LOD	34	5.30E-07	-1.10E-03
P-B	Sept-18	1.44E-06	n.m	6.29E-09	<LOD	1.14E-05	1.05E-06	3.89E-04	2.55E-06	1.34E-07	34	-	-1.52E-03
P-B	Dec-18	2.76E-06	7.82E-07	6.09E-09	<LOD	9.23E-06	2.07E-05	3.43E-04	8.70E-07	<LOD	37	1.75E-05	-9.76E-04

P-LAV	Apr-18	7.64E-05	1.15E-07	6.35E-09	8.92E-08	1.47E-05	4.55E-07	4.36E-04	4.08E-06	<LOD	30	2.54E-06	-2.43E-03
P-LAV	Sept-18	8.30E-06	n.m	5.88E-09	<LOD	1.30E-05	1.18E-06	4.51E-04	4.33E-06	1.94E-07	35	-	-2.62E-03
P-LAV	Dec-18	2.26E-05	2.25E-07	6.07E-09	<LOD	1.19E-05	9.04E-07	4.00E-04	3.94E-06	1.09E-07	34	5.02E-06	-1.95E-03
P-SOA	Apr-18	2.27E-05	6.79E-08	8.13E-09	6.58E-07	1.76E-05	6.63E-07	5.45E-04	5.01E-06	<LOD	31	1.48E-06	-9.44E-04
P-SOA	Sept-18	3.10E-06	n.m	5.69E-09	4.55E-10	1.18E-05	2.25E-06	4.18E-04	3.79E-06	6.83E-08	35	-	-2.42E-03
P-SOA	Dec-18	3.69E-05	2.34E-07	6.07E-09	<LOD	1.22E-05	6.10E-07	4.14E-04	4.30E-06	2.29E-07	34	5.22E-06	-2.10E-03
PUZ-F	Apr-18	1.23E-03	2.94E-08	9.52E-09	<LOD	2.01E-05	2.91E-07	7.53E-04	9.58E-04	1.42E-04	38	6.12E-07	3.10E-04
PUZ-F	Sept-18	8.79E-04	n.m	9.35E-09	<LOD	1.63E-05	9.68E-07	6.97E-04	8.81E-04	1.50E-04	43	-	1.28E-03
PUZ-F	Dec-18	9.81E-04	3.15E-08	8.96E-09	<LOD	1.77E-05	2.67E-07	7.57E-04	9.15E-04	1.41E-04	43	6.60E-07	2.33E-04
PUZ-N	Sept-18	1.06E-03	n.m	6.83E-09	<LOD	1.21E-05	2.40E-07	4.81E-04	1.93E-04	1.06E-03	40	-	-9.04E-04
CAM-F	Apr-18	3.55E-04	8.76E-09	2.53E-09	<LOD	8.91E-06	3.61E-07	2.51E-04	1.00E-03	3.12E-05	28	1.87E-07	-6.00E-03
CAM-F	Sept-18	2.40E-04	n.m	2.01E-09	1.33E-08	7.17E-06	2.79E-07	2.26E-04	2.13E-03	4.41E-05	32	-	-6.24E-03
CAM-F	Dec-18	3.10E-04	9.22E-09	3.80E-09	2.17E-08	8.28E-06	2.25E-07	2.84E-04	1.89E-03	3.71E-05	34	1.87E-07	-3.93E-03

Table 4: CFC and SF_6 concentrations measured in water in pmol/L and pptv.

SPRINGS CODE	SF6		CFC-12		CFC-11		CFC-113	
	pmol/L	pptv	pmol/L	pptv	pmol/L	pptv	pmol/L	pptv
FORC	8.39E-04	2.75	1.23E-01	30.23	1.34	88.03	0.00E+00	-
S-SOT	1.65E-03	5.41	6.78E-01	166.82	3.22	211.58	5.88E-02	12.84
P-B	0.00E+00	-	3.14E-01	67.32	4.54	253.58	0.00E+00	-
P-LAV	5.83E-04	1.71	1.11E-01	23.86	2.45	137.02	2.08E-02	3.78
PUZ-F	0.00E+00	-	8.01E-02	19.00	2.27	143.51	8.68E-02	18.27
CAM-F	2.81E-04	0.89	1.95E-01	46.24	4.47	283.04	5.20E-02	10.95
FONT	2.64E-03	8.33	8.03E-02	19.06	2.11	133.45	2.26E-02	4.75

Abstract

The varied gaseous composition of thermo-mineral waters emerging in a non-active zone reflects the diversity and complexity of groundwater pathways and provides important insights into their hydrogeological behaviours. The investigated geochemical content of complex thermo-mineral springs revealed the need to use dissolved gas contents as part of a multi-tracer approach to discriminate processes, geogenic (water-gas-rock interactions), abiotic (geological confinement, flow paths) and biotic activity influencing geochemical of groundwater along regional pathways. Irrespective of the dissolved element content or the water type, examining the overall concentration of dissolved gases enables an effective delineation of regional groundwater flow paths. Using dissolved gas content further contributed to the circumvention of some analytical challenges associated with conventional isotopic or geochemical techniques, often linked to the high concentration of elements such as iron, sulfate, sulfide or other naturally occurring elements content. The primary objectives are to analyse the gas composition of individual springs, to identify the origin of these gases in the groundwater, and to use this gas composition to improve the understanding of the flow patterns contributing to the geochemical diversity observed at the surface of the groundwater. From field investigations in a geologically and structurally complex area of Eastern Corsica (France), three types of gas contents are identified: (type 1) CH_4 & H_2S-rich, (type 2) N_2-rich and (type 3) CO_2-rich. The study of these dissolved gases highlights that the wide geochemical diversity of thermo-mineral waters observed here is not only related to the mineralogical composition of the local aquifer but also involves strong and cumulative interactions along deep regional circulation pathways. This approach also reveals a common deep crustal gaseous influence characterised by N_2 production, which interacts during up flow with groundwater and then with the local metamorphic or sedimentary rock matrix. The groundwater's isotopic and geochemical contents are then altered by local lithologies encountered through both abiotic and biotic interactions. Finally, at shallow depths, phreatic groundwater can add its geochemical and isotopic footprint and dilute this complex mixture before groundwater emerges as mineral spring. This paper answers the primary objectives yet further demonstrates that using dissolved gas as a tracer of groundwater flow paths allows a deeper interpretation of surface geochemical and isotopic observations, distinguishes local from regional flow paths, and provides information about processes at the origin of groundwater diversity.

The combination of tools presented in this paper (i.e., geochemical, dissolved gas, and isotopic tools) allows the establishment of a reliable regional groundwater flow scheme for thermo-mineral waters in a non-active zone. This scheme is essential to improve thermo-mineral water management, and protection to ensure their sustainable quality in front of increasing anthropogenic and climatic pressures.

Keywords

Hydrogeology, thermo-mineral waters, water stable isotopes, water-rock interactions, dissolved gases (CO_2, CH_4, H_2S, N_2, He).

Highlights

- geogenic processes combined with biotic activity generate diversified mineral waters
- CO_2, N_2 and CH_4 are most widely represented dissolved gases in mineral waters
- excess air can be used as tracer of biotic processes
- complex regional mineral water flows are identified
- an improved regional hydrogeological conceptual model is proposed

Declaration of interests

☒ The authors declare that they have no known competing financial interests or personal relationships that could have appeared to influence the work reported in this paper.

☐ The authors declare the following financial interests/personal relationships which may be considered as potential competing interests:

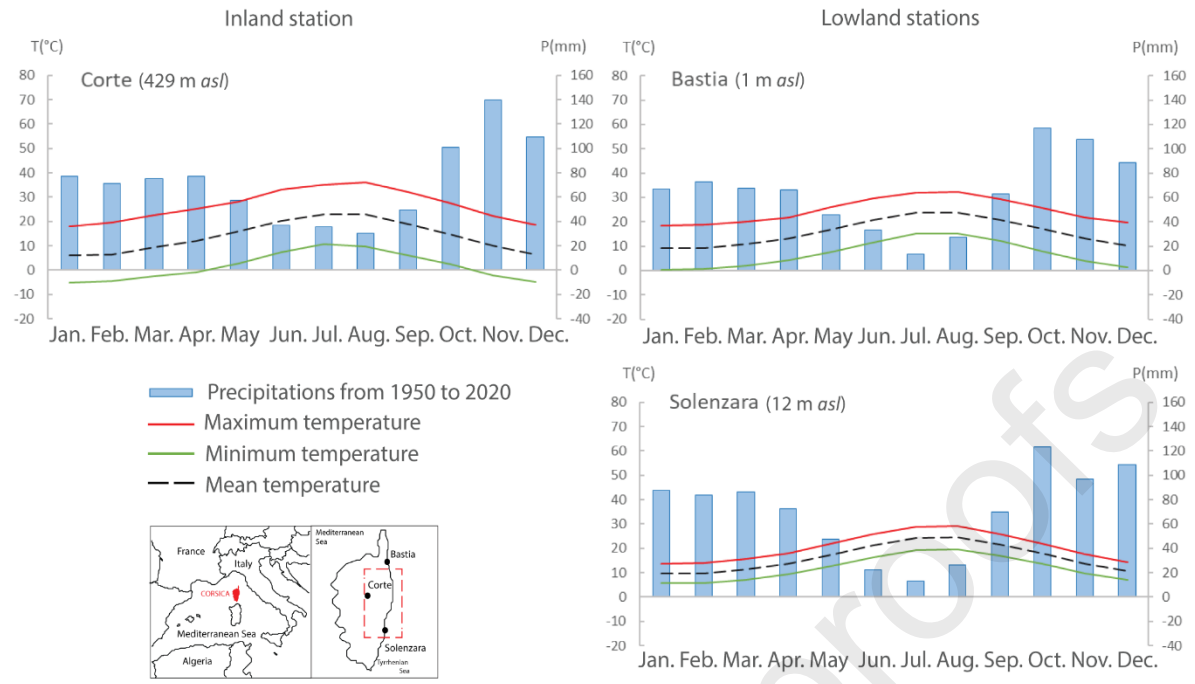

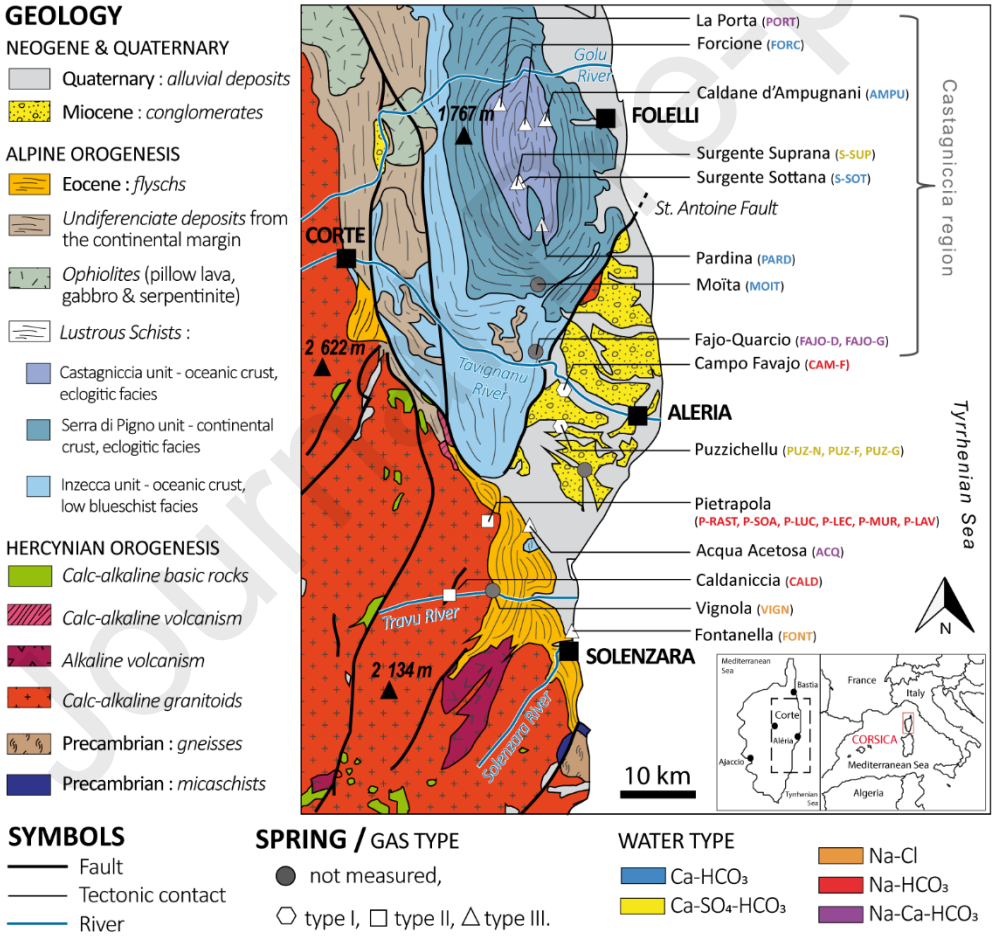

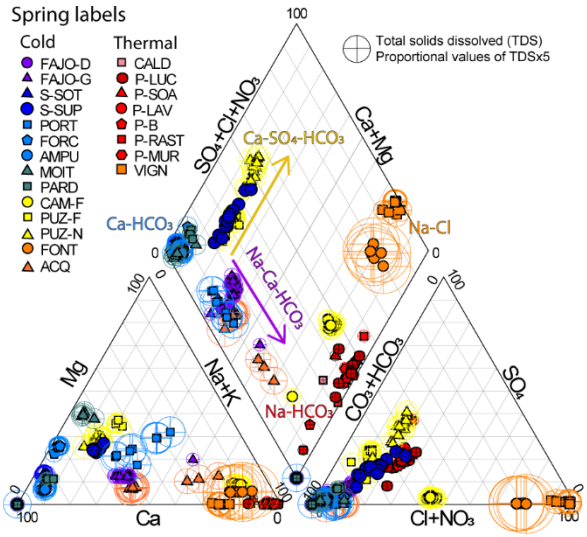

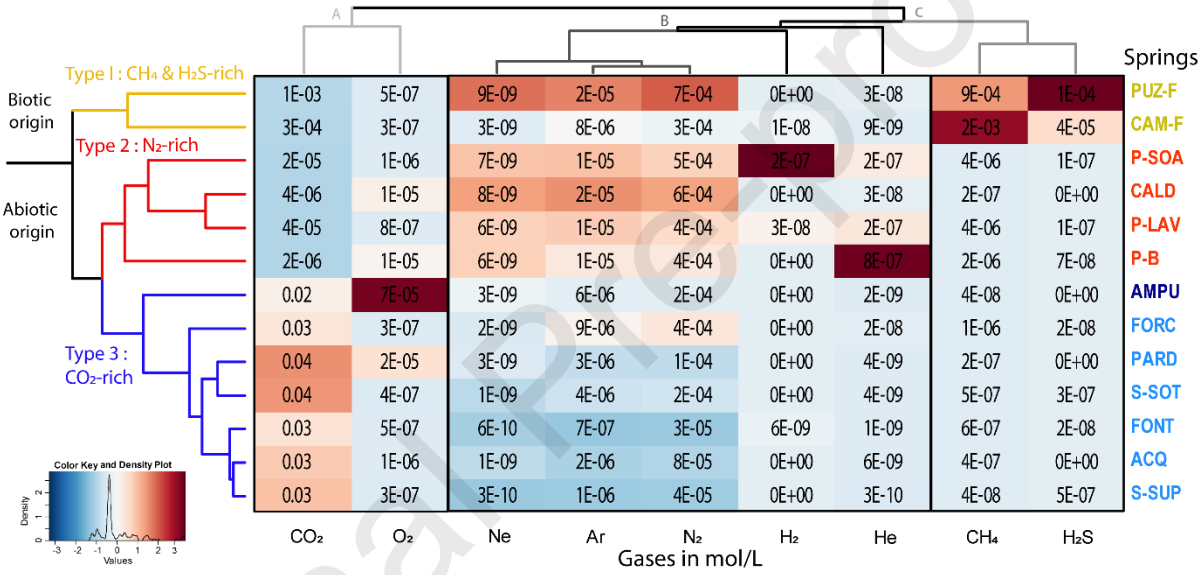

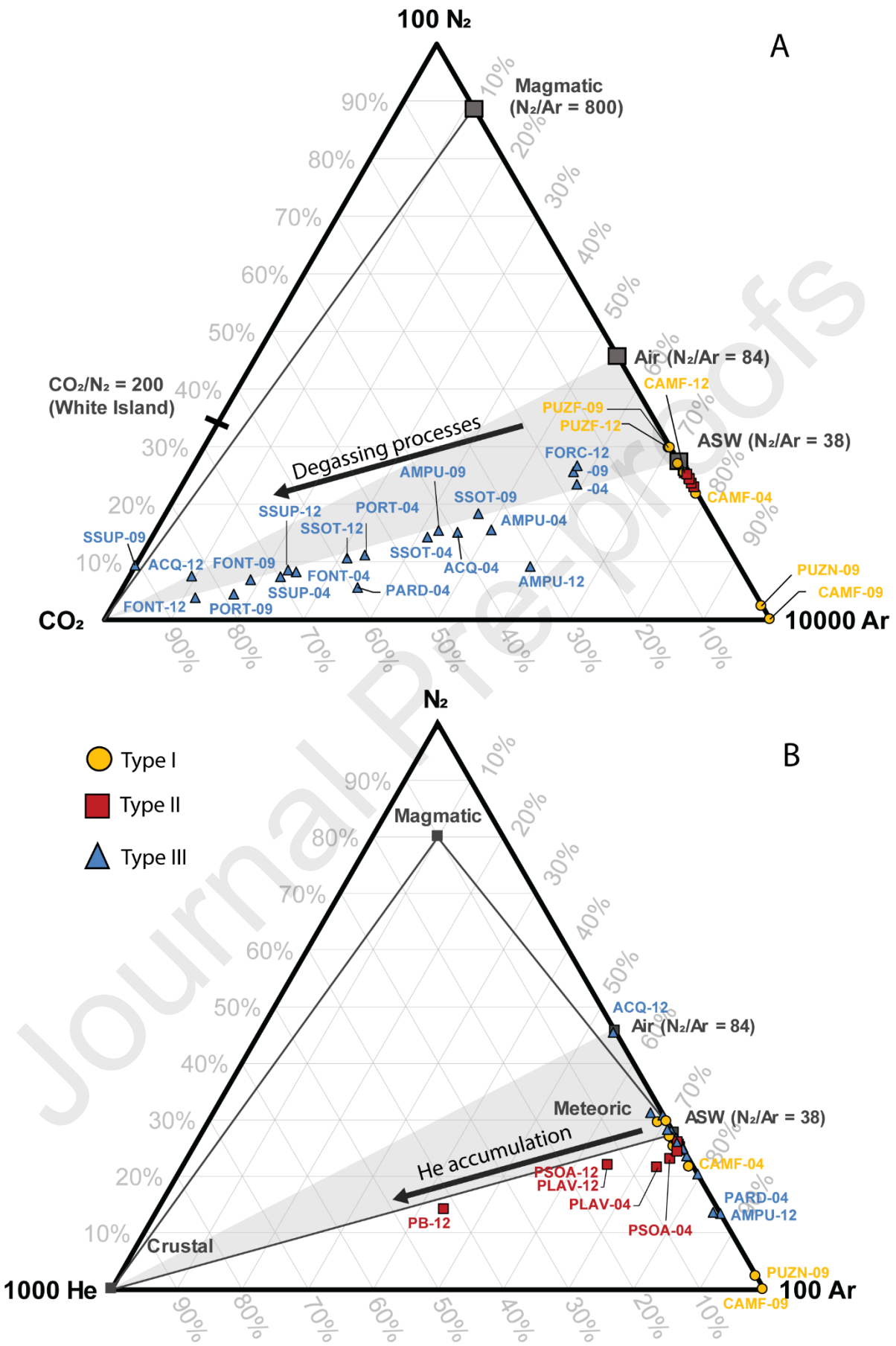

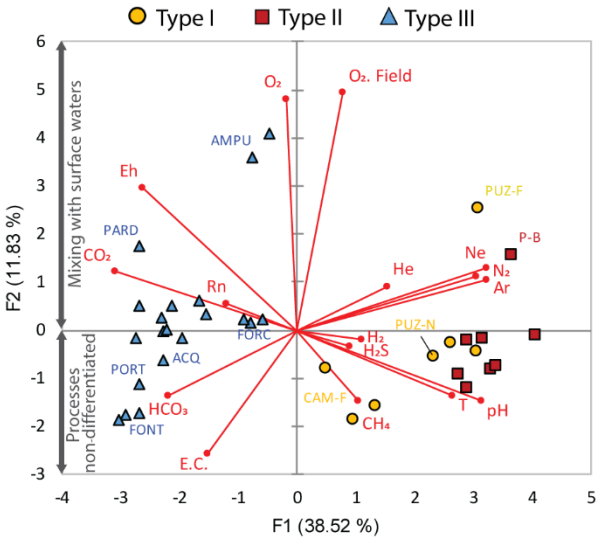

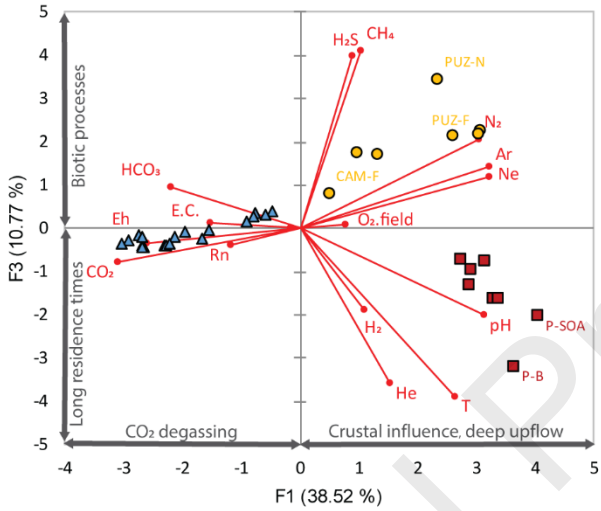

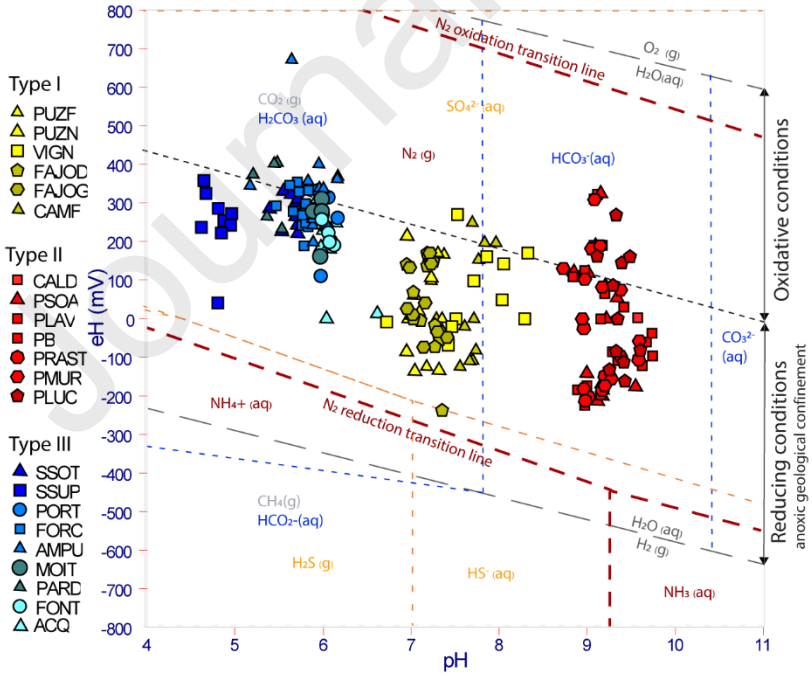

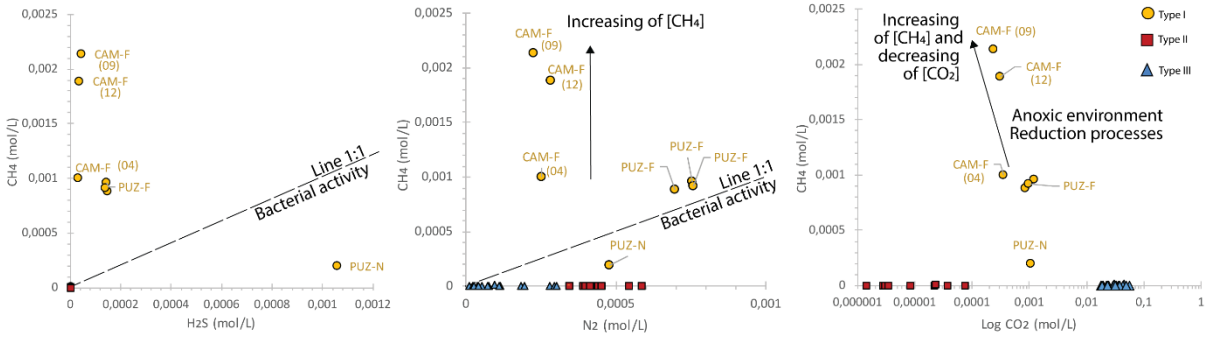

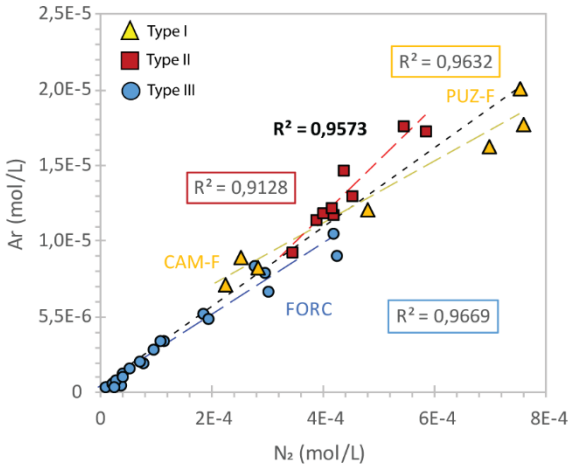

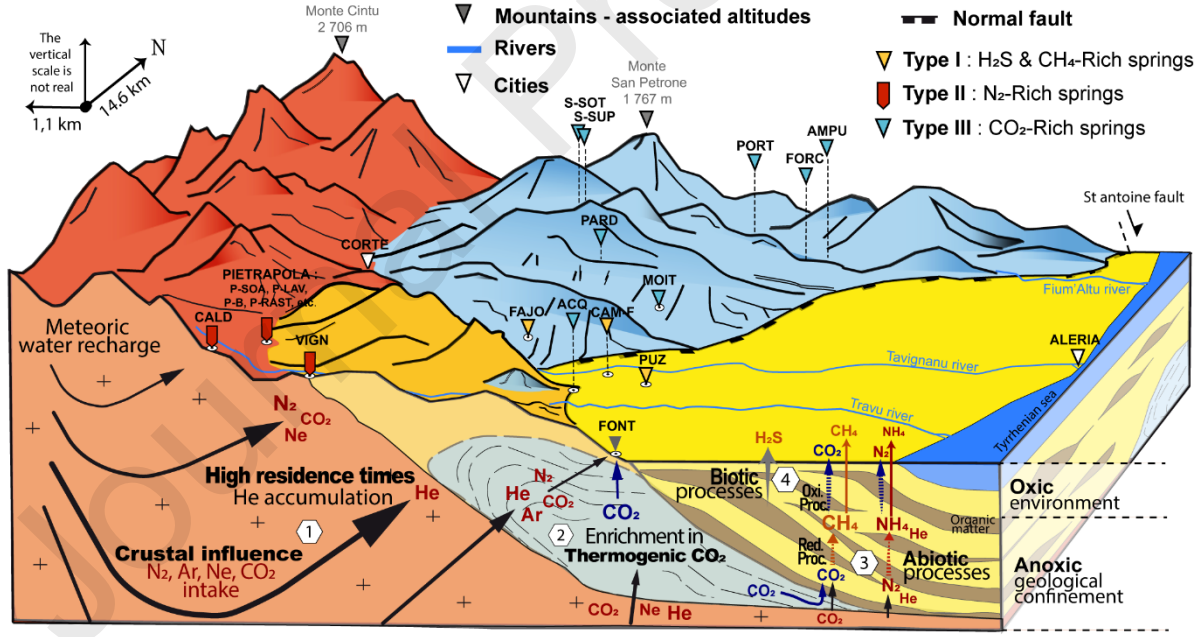

1 **Crustal influence** : enrichment in **N₂, Ar, Ne & CO₂** - Type II

2 **Thermogenic processes** : enrichment in **CO₂**, due to re-mobilisation of thermogenic **CO₂** according to water interraction with metamorphised rocks - Type III

3 **Geogenic processes** : Influence of anoxic geological confinement on water, the very reducing aquifer conditions leads to reduce **CO₂** into **CH₄** and the **N₂** into **NH₄** - Type I

4 **Biotic processes :** the bacterial activity in organic matter-rich environment leads to consum **CH₄** and sulfate to produce **CO₂** and **H₂S** - Type I

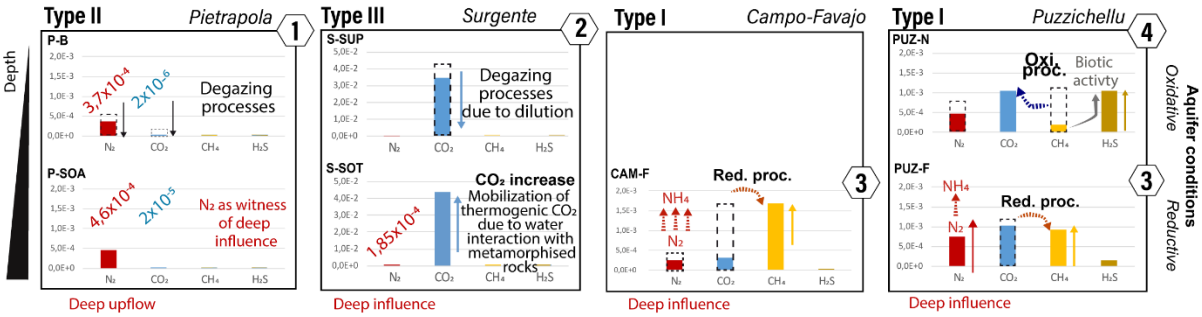

1 **Crustal influence** : enrichment in **N_2, Ar, Ne & CO_2** - Type II

2 **Thermogenic processes** : enrichment in **CO_2**, due to re-mobilisation of thermogenic **CO_2** according to water interraction with metamorphised rocks - Type III

3 **Geogenic processes** : Influence of anoxic geological confinement on water, the very reducing aquifer conditions leads to reduce **CO_2** into **CH_4** and the **N_2** into **NH_4** - Type I

4 **Biotic processes** : the bacterial activity in organic matter-rich environment leads to consum **CH_4** and sulfate to produce **CO_2** and **H_2S** - Type I